Joint Optimization Schemes for Cooperative Wireless Information and Power Transfer over Rician Channels

Joint Optimization Schemes for Cooperative Wireless Information and Power Transfer over Rician Channels

Deepak Mishra, Swades De, and Carla-Fabiana Chiasserini

***Abstract*—Simultaneous wireless information and power transfer (SWIPT) can lead to uninterrupted network operation by integrating radio frequency (RF) energy harvesting with data communication. In this paper, we consider a two-hop source-relay-destination network and investigate the efficient usage of a decode-and-forward (DF) relay for SWIPT toward the energy-constrained destination. In particular, by assuming a Rician fading environment, we jointly optimize power allocation (PA), relay placement (RP), and power splitting (PS) so as to minimize outage probability under the harvested power constraint at the destination node. We consider the two possible cases of source-to-destination distance: (i) small distance with direct information transfer link; and (ii) relatively large distance with no direct reachability. Analytical expressions for individual and joint optimal PA, RP, and PS are obtained by exploiting convexity of outage minimization problem for the no direct link case. In case of direct source-to-destination link, multi-pseudoconvexity of joint-optimal PA, RP, and PS problem is proved, and alternating optimization is used to find the global optimal solution. Numerical results show that the joint optimal solutions, although strongly influenced by the harvested power requirement at the destination, can provide respectively 64% and 100% outage improvement over the fixed allocation scheme for without and with direct link.**

***Index Terms*—RF energy harvesting; Rician fading; decode and forward; power allocation; relay placement; power splitting ratio; outage-harvested power tradeoff; alternating optimization.**

I. Introduction and Background

Relay-assisted data communication and cooperative transmission strategies offer significant benefits over the direct source-to-destination transmission. The advantages include cooperative diversity, energy saving, increased secrecy, network coverage extension, and improvement of quality-of-service in wireless networks. Moreover, cooperative relaying techniques can overcome high path-loss, blocking or shadowing losses, and high transmit power requirements, by providing alternate path(s) from source to destination via one or more relays. There are several studies on optimal power allocation (PA) and relay placement (RP) for cooperative amplify-and-forward (AF) as well as decode-and-forward (DF) information relaying under different fading conditions [1]–[6]. Minimization of source-sum-power subject to outage constraints using DF relay is studied in [7] and [8], respectively with as well as without direct links between multiple sources and single destination.

D. Mishra and S. De are with the Department of Electrical Engineering and Bharti School of Telecommunication, Indian Institute of Technology Delhi, New Delhi, India (e-mail: {deepak.mishra, swadesd}@ee.iitd.ac.in). C.-F. Chiasserini is with Politecnico di Torino, Torino, Italy, and is also a Research Associate with the Institute of Electronics, Computer and Telecommunication Engineering of the National Research Council of Italy (IEIIT-CNR), Torino, Italy (e-mail: chiasserini@polito.it).

Another line of research that has recently emerged is radio frequency (RF) energy harvesting (RFEH) at the energy-constrained field nodes, which can prolong the lifetime of wireless networks. Since most of the long-range communication is based on transmission of RF signals, usage of this RF radiation for energy harvesting leads to simultaneous wireless information and power transfer (SWIPT) to the energy-constrained receiver. SWIPT is discussed in the pioneering works [9], [10]. The study in [11] introduces two mechanisms for practical implementation of SWIPT: a) power splitting (PS) and b) time switching (TS). Subsequently, PS-based and TS-based routing protocols for RFEH AF relay node and single source-destination $(\mathcal{S}-\mathcal{D})$ pair are proposed in [12]. A dual-hop RFEH AF relaying system, with and without the presence of co-channel interference is investigated in [13]. PA strategies for RFEH DF relay for multiple $\mathcal{S}-\mathcal{D}$ pairs are proposed in [14]. The performance of a dual-hop RFEH full-duplex relaying system is studied in [15] for both AF and DF relaying protocols. Authors in [15], also investigated optimal TS ratio under different communication modes. SWIPT without as well as with cooperative energy relaying is discussed in [16], and the impact of spatial randomness of relay locations on the performance of SWIPT is studied in [17]. The work in [18] demonstrated that there exists a trade-off between information and energy transfer for relay selection in SWIPT, as the preferable relay position is different for information transfer and energy transfer. Yet, optimal PA and RP are not considered in [12]–[18]. It is worth noting that [12]–[15] consider source-relay and relay-destination distances as constants, whereas [16]–[18] consider relay selection strategies. Also, the optimal PA and RP problem investigated in [1]–[8] for two-hop information relaying, do not consider the Rician fading model, which is more appropriate to incorporate the effect of strong line-of-sight (LOS) component in SWIPT [19], [20] and information relaying systems [21].

Accounting for the system and wireless device constraints, it is argued in [22] that multi-hop RF energy transfer can improve RFEH efficiency by deploying relay nodes close to the target energy receiver. In this technique, the relay first collects the otherwise-dispersed RF energy of the source and then transfers it to the energy receiver, which reduces path loss and improves RF-to-DC conversion efficiency due to a higher received power [23]. Two-hop RF energy transfer and multi-path energy routing have been experimentally demonstrated recently in [23] and [24]. These works however have not looked into joint information and RF energy transfer aspects.

TABLE I: Joint cooperative optimization schemes for SWIPT.

Optimization scheme	Practical setting	Node(s) where optimization is performed
Optimal PA	$\mathcal{S}$ and $\mathcal{R}$, connected to the common power grid or having common energy resource, cooperate to share the total power budget optimally	$\mathcal{S}$ or $\mathcal{R}$
Optimal RP	When there are no terrain asperities or blockage, $\mathcal{R}$ can adjust, or can be instructed by $\mathcal{S}$ to adjust, its position optimally to aid efficient SWIPT to $\mathcal{D}$	$\mathcal{R}$ or $\mathcal{S}$
Optimal PS	RFEH $\mathcal{D}$ has enough energy resources to carry out the PS optimization	$\mathcal{D}$
Joint-optimal	It has the luxury of combining the merits of all three optimization schemes	$\mathcal{S}$, $\mathcal{R}$, and $\mathcal{D}$

Intuitively, optimal PA and RP in SWIPT are quite different from those in conventional information transfer [1]–[8], where RF energy transfer using relay is not considered.

In this paper we study the performance in terms of outage probability of a two-hop, half-duplex DF relay-assisted SWIPT with a single source $\mathcal{S}$ and destination $\mathcal{D}$. We consider the two possible cases: (i) relatively short $\mathcal{S}$-to-$\mathcal{D}$ distance where $\mathcal{D}$ is capable of receiving information directly from $\mathcal{S}$; and (ii) long $\mathcal{S}$-to-$\mathcal{D}$ distance, with no direct communication link [2]–[6]. However, in both cases $\mathcal{D}$ is not capable of harvesting energy from $\mathcal{S}$ due to low RF energy transfer range [23]. $\mathcal{S}$ and relay $\mathcal{R}$ are assumed to have enough energy resources, whereas $\mathcal{D}$ operates with the harvested RF energy from the received signal from $\mathcal{R}$ using the PS technique. To improve the efficiency of DF relay-assisted SWIPT for a given $\mathcal{S}-\mathcal{D}$ pair, we propose four different optimization schemes under varying real-world constraints (practical settings), as mentioned in Table I. The table also underlines at which node(s) the optimization is performed. The practical settings for the problem considered include self-sustainable broadcasting networks and multiuser downlink SWIPT systems, where the user devices are battery constrained, whereas the broadcasting base station and the relay are connected to the power grid [18]. $\mathcal{S}$ and $\mathcal{R}$ can also be considered as infrastructure nodes in network-assisted device-to-device (D2D) communications or Long-Term Evolution (LTE) Advanced system, which share the total power for efficient information and energy transfer to the nearby battery-constrained wireless devices.

To the best of our knowledge, this is the first work that presents a joint optimization of PA, RP, and PS for SWIPT to minimize the outage probability at $\mathcal{D}$ without and with direct communication link from $\mathcal{S}$. To incorporate the effect of strong LOS component in SWIPT, outage performance analysis is done using Rician fading model, which has not been considered before. While minimizing outage probability p_{out}, we consider constraints on total transmit power $P_{_T}$ (sum of $\mathcal{S}$ and $\mathcal{R}$ power) and required harvested power ζ_P at $\mathcal{D}$. Our key contributions are as follows.

- Joint optimization schemes for cooperative SWIPT to enhance outage performance of $\mathcal{R}$-assisted $\mathcal{S}$-to-$\mathcal{D}$ communication are presented for both without and with $\mathcal{S}$-to-$\mathcal{D}$ direct link. All optimization results are derived under practical RFEH constraints at $\mathcal{D}$, while considering the Rician channel fading to incorporate the dominant LOS component of the links. The results for Rayleigh fading can be easily generated by setting the Rice factor value as zero.
- In SWIPT with no direct $\mathcal{S}$-to-$\mathcal{D}$ link, analytical expressions are obtained for both individual and joint-optimal PA, RP, and PS to minimize p_{out}, subject to $P_{_T}$ and ζ_P constraints.
- For short $\mathcal{S}$-to-$\mathcal{D}$ distance with direct communication link between $\mathcal{S}$ and $\mathcal{D}$, tri-pseudoconvexity of p_{out} is proved. Subsequently, for individual PA, RP, and PS optimization, semi-closed-form solutions are obtained by exploiting individual pseudoconvexity of p_{out} with respect to PA, RP, and PS. The joint-optimal solution is obtained by using alternating optimization technique along with bi-pseudoconvexity of p_{out} with optimized PS in P_s and d.
- Impact of RFEH requirement at $\mathcal{D}$ on optimal PA, RP, and PS for efficient SWIPT is discussed via numerical results. Improved performance of the proposed joint and individual optimization schemes over non-cooperative fixed allocation scheme is also demonstrated. For example, with respect to fixed allocation scheme, joint optimization offers about 64% and 100% improvement in p_{out} for without and with direct $\mathcal{S}$-to-$\mathcal{D}$ link, respectively.
- Trade-off between p_{out} and ζ_P is investigated in the proposed joint optimization scheme under different Rice factor values. The impacts of transmit power budget, $\mathcal{S}$-to-$\mathcal{D}$ distance, and channel conditions on optimized solutions and minimized p_{out} are also studied.

The rest of the paper is organized as follows. Network topology considered and its motivation are discussed in Section II. Problem definition is presented in Section III. Optimal PA for fixed RP and PS, without and with direct $\mathcal{S}$-to-$\mathcal{D}$ link availability is presented in Section IV. Section V contains analytical solutions for optimal RP with predetermined PA and PS for both short and long $\mathcal{S}$-to-$\mathcal{D}$ distance cases. PS ratio optimization is studied in Section VI. Joint-optimal PA, RP, and PS scheme, exploiting convexity and multi-pseudoconvexity of p_{out} respectively for no direct link and with $\mathcal{S}$-to-$\mathcal{D}$ direct link, are analyzed in Section VII. Numerical results are presented in Section VIII, which is followed by the concluding remarks in Section IX.

II. System model

Here we discuss the network and channel models along with motivation for these consideration.

A. Network topology and channel model

We consider a three-node, two-hop wireless network, consisting of an information source $\mathcal{S}$, a relay node $\mathcal{R}$, and a destination node $\mathcal{D}$ placed on a two-dimensional Euclidean plane. We consider two system models for RP, depending on the availability of direct $\mathcal{S}$-to-$\mathcal{D}$ communication link: *linear* and *elliptical*. In the first case (Fig. 1(a)), when D is reasonably large, there is no direct $\mathcal{S}$-to-$\mathcal{D}$ link available due to large path loss, shadowing, and fading effects. Hence, here $\mathcal{R}$ is placed on the LOS path between $\mathcal{S}$ and $\mathcal{D}$ to maximize the gain from relaying. In the second case, with direct $\mathcal{S}$-to-$\mathcal{D}$ link availability (Fig. 1(b)), $\mathcal{R}$ is placed at a position along the locus of the ellipse [6], [25] to avoid the obstruction to direct $\mathcal{S}$-to-$\mathcal{D}$ link. $\mathcal{S}$ and $\mathcal{D}$, separated by a distance D, are located at the two foci of the ellipse.

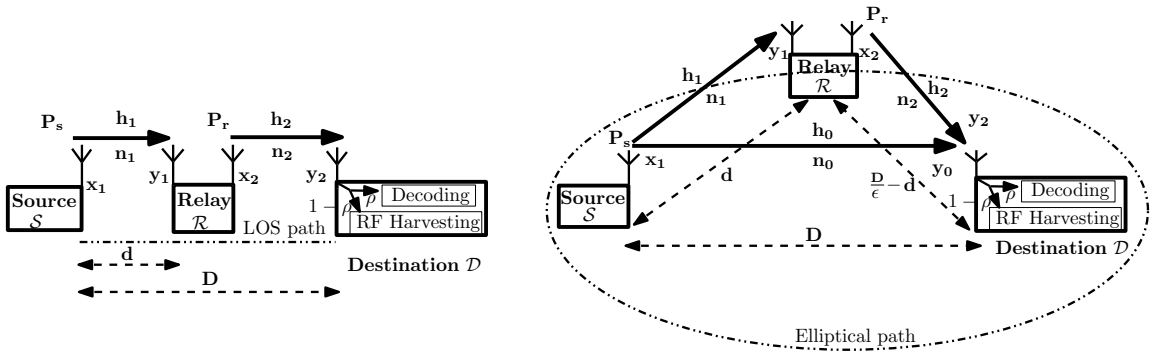

(a) Relay placement on linear LOS path for large $\mathcal{S}$-to-$\mathcal{D}$ distance with no direct $\mathcal{S}$-to-$\mathcal{D}$ link

(b) Relay placement on elliptical path for short $\mathcal{S}$-to-$\mathcal{D}$ distance with direct $\mathcal{S}$-to-$\mathcal{D}$ link availability

Fig. 1: Three-node network topology with two $\mathcal{S}$-to-$\mathcal{D}$ distance-based cases. $\mathcal{R}$ has two directional antennas: one directed toward $\mathcal{S}$ and the other directed toward $\mathcal{D}$.

$\mathcal{R}$ operates in half-duplex DF mode. Thus, the information transfer occurs in two slots: in the first slot from $\mathcal{S}$ to $\mathcal{R}$ (and $\mathcal{S}$ to $\mathcal{D}$ if direct $\mathcal{S}$-to-$\mathcal{D}$ link is available), and in the second slot from $\mathcal{R}$ to $\mathcal{D}$. It may be noted that, although the intended half-duplex operation could be conducted using single omnidirectional antenna at each node as in conventional cooperative communication systems, we consider two directional antennas at $\mathcal{R}$ (Fig. 1). One is directed towards $\mathcal{D}$ – essentially for efficient $\mathcal{R}$-to-$\mathcal{D}$ energy transfer (or SWIPT), and the other is directed towards $\mathcal{S}$ for effective $\mathcal{S}$-to-$\mathcal{R}$ information transfer.

Indeed, $\mathcal{D}$ has RFEH capability. The RFEH operation is based on PS technique [11], in which the received power is split into two parts with a PS ratio $\rho \in (0,1)$. A fraction ρ of the received power at $\mathcal{D}$ is used for data detection or decoding, and the remaining fraction $(1-\rho)$ is used for RFEH. For simplicity, an ideal PS is assumed, neglecting the power loss, noise degradation, and synchronization errors. The received signal y_0 at $\mathcal{D}$ and y_1 at $\mathcal{R}$ from $\mathcal{S}$ in the first slot, and y_2 at $\mathcal{D}$ from $\mathcal{R}$ in the second slot are given by:

$$y_0 = h_0\sqrt{P_s}x_1 + n_0, \quad y_1 = h_1\sqrt{P_s}x_1 + n_1, \quad y_2 = h_2\sqrt{P_r}x_2 + n_2 \tag{1}$$

where n_0, n_1, and n_2 are mutually independent Additive White Gaussian Noise (AWGN) at the respective receivers, with zero mean and same noise power N_0. P_s and P_r are the transmit powers of $\mathcal{S}$ and $\mathcal{R}$, respectively, with $P_{_T} = P_s + P_r$ as the total transmit power budget. x_1 and x_2 are the signals transmitted by $\mathcal{S}$ and $\mathcal{R}$, respectively. We also assume that $\mathbb{E}[x_i] = 0$ and $\mathbb{E}[|x_i|^2] = 1, \forall i \in \{1,2\}$. h_0, h_1, and h_2 are the Rician channel gain coefficients. Over Rician fading channels, the instantaneous signal-to-noise ratio (SNR) γ_0 for $\mathcal{S}$-to-$\mathcal{D}$ link, γ_1 for $\mathcal{S}$-to-$\mathcal{R}$ link, and γ_2 for $\mathcal{R}$-to-$\mathcal{D}$ link are distributed according to the weighted noncentral-χ^2 distribution with two degrees of freedom, whose cumulative distribution function (CDF) is given by [26]:

$$F_{\gamma_i}(\gamma) = 1 - \mathcal{C}_{\gamma_i}(\gamma) = 1 - Q_1\left(\sqrt{2K_i}, \sqrt{\frac{2(K_i+1)\gamma}{\overline{\gamma_i}}}\right) \tag{2}$$

where $\mathcal{C}_{\gamma_i}(\cdot)$ is the complimentary CDF of γ_i and $Q_1(\cdot,\cdot)$ is the first order Marcum Q-function [26]. K_i is the Rice factor defined as the ratio of power of LOS component to the scattered components. $\overline{\gamma_i} = \mathbb{E}[\gamma_i]$ is the average SNR of the respective links, given by: $\overline{\gamma_0} = \frac{a_d P_s}{N_0 D^l}$, $\overline{\gamma_1} = \frac{a_s P_s}{N_0 d^l}$, and $\overline{\gamma_2} = \frac{a_r P_r}{N_0(\frac{D}{\epsilon}-d)^l}$, where d and $\left(\frac{D}{\epsilon}-d\right)$ are $\mathcal{S}$-to-$\mathcal{R}$ and $\mathcal{R}$-to-$\mathcal{D}$ distances, respectively. ϵ is the eccentricity; $\epsilon = 1$ for linear case (cf. Fig. 1(a)) when there is no direct $\mathcal{S}$-to-$\mathcal{D}$ link available. a_d, a_s, and a_r account for the channel parameters, namely, fading and antenna gains, in the respective link, and l is the path loss exponent. The average harvested power at $\mathcal{D}$ is $P_{_D}^H = \frac{\eta a_r (1-\rho) P_r}{\left(\frac{D}{\epsilon}-d\right)^l}$, where η is the RF-to-DC conversion efficiency of the RFEH circuitry at $\mathcal{D}$.

B. Motivation for proposed system model

Our consideration of Rician fading channel model is motivated by the fact that, there is a presence of strong LOS component in practical SWIPT and information relaying scenarios with direct link availability or short communication ranges. Following this, we have employed a commonly used elliptical topology [6], [25] for RP which helps to extend the conventional line topology to a more generic two-dimensional RP model, while considering the possibility of a direct LOS path between $\mathcal{S}$ and $\mathcal{D}$. Also, it offers flexibility in realization of a realistic non-blocking model that incorporates the behavior of practical directional antennas having reduced gains with increase in angle away from the direction of main beam [27]. Hence, it allows $\mathcal{R}$ (the blocking object) to come closer to $\mathcal{S}$ and $\mathcal{D}$ (transmitting and receiving directional antennas) from the perpendicular direction, yet stay far away from the direction of the main beam.

In optimal power (system resource) allocation, if independent transmit power budgets $P_{_{T_\mathcal{S}}}$ and $P_{_{T_\mathcal{R}}}$ are considered at $\mathcal{S}$ and $\mathcal{R}$ respectively, minimum p_{out} will trivially occur at full power utilization $\left(P_s = P_{_{T_\mathcal{S}}}, P_r = P_{_{T_\mathcal{R}}}\right)$. Instead, we consider controlled relaying where $\mathcal{S}$ and $\mathcal{R}$ are either administered by the same service provider, or have a common energy resource that they share for efficient SWIPT to $\mathcal{D}$. One such practical setting includes $\mathcal{S}$ being a base station in a cellular scenario with $\mathcal{R}$ as a network operator controlled relay node. So, in our PA optimization, we consider a joint total transmit power budget $P_{_T} = P_s + P_r$ and optimally distribute it between $\mathcal{S}$ and $\mathcal{R}$ to minimize p_{out}, which is also influenced by RP.

It is also worth noting that, in the proposed system model information transfer from $\mathcal{S}$-to-$\mathcal{D}$ is over two hops in addition to the possible direct $\mathcal{S}$-to-$\mathcal{D}$ communication link, whereas the energy is transferred via only one hop, from $\mathcal{R}$-to-$\mathcal{D}$. Two-hop energy transfer is not considered because of very

low RFEH sensitivity [28], which leads to a very low RF energy transfer range as compared to the typical wireless data communication range [23], [24]. Hence, for a typical $\mathcal{S}$-to-$\mathcal{D}$ information transfer distance and with the current state of RFEH technology [28], for practical feasibility of RFEH at $\mathcal{D}$, the transmit power P_s at $\mathcal{S}$ has to be very large. The Effective Isotropic Radiated Power (EIRP) required at $\mathcal{S}$ in order to have ζ_P amount of DC power available after RF-to-DC conversion at $\mathcal{D}$ is given by: EIRP $\triangleq P_s G_s = \frac{\zeta_P}{\eta(1-\rho)G_D}\left(\frac{4\pi D f}{c}\right)^l$, where G_s and G_D are the antenna gains of $\mathcal{S}$ and $\mathcal{D}$, respectively, c is the speed of light, and f is the frequency of the transmitted signal. Considering two values of ζ_P as 0 dBm and 10 dBm for RFEH at $\mathcal{D}$ using commercially-available Powercast RF harvester and antennas [29], $\rho = 0.01$, $D = 10$ m, $G_s = G_D = 6.1$ dBi, $f = 915$ MHz, and $l = 3$, the EIRP required is at least 23.35 kW and 198.55 kW, respectively. Thus, even at very low D, the transmit power requirements are much higher than the maximum transmit power limits defined by FCC regulations in different frequency bands. For example, at 900 MHz band the allowable maximum EIRP is 4 W [30].

At last, we comment on the practical reference scenarios for the system setting considered in the paper. As noted in [9]–[19], a SWIPT-enabled network can overcome the finite lifetime limitation of battery-driven nodes, or high energy and infrastructure cost involved with the networks that are connected to the power grid. So, in order to enhance the practical applicability of SWIPT under different real-world constraints, we have proposed four optimization schemes, as mentioned in Table I. These optimization schemes can be employed individually or jointly, depending on the underlying reference scenario. For example, if we have a central controller for PA to $\mathcal{S}$ and $\mathcal{R}$, no terrain blockage for RP, and PS optimization capability at $\mathcal{D}$, all three parameters (PA, RP, and PS) can be jointly optimized. The proposed optimization is performed by the node(s) with the help of full channel state information (CSI) acquired by (i) $\mathcal{R}$ for $\mathcal{S}$-to-$\mathcal{R}$ link, (ii) $\mathcal{D}$ for $\mathcal{R}$-to-$\mathcal{D}$ link, and (iii) $\mathcal{D}$ for $\mathcal{S}$-to-$\mathcal{D}$ link, from the pilot signals sent by $\mathcal{S}$, $\mathcal{R}$, and $\mathcal{S}$, respectively. This collected CSI is fed back to the node which performs the optimization. Intuitively, the joint optimization scheme requires the most signaling cost due to the involvement of all three nodes, i.e., $\mathcal{S}$, $\mathcal{R}$, and $\mathcal{D}$, in the cooperative optimization of PA, RP, and PS to realize minimum p_{out} for a given total power budget P_T, $\mathcal{S}$-to-$\mathcal{D}$ distance, and energy demand ζ_P at $\mathcal{D}$.

III. Problem Definition

We now derive outage probability expressions and present the proposed optimization framework.

A. Outage probabilty analysis

The outage probability p_{out}, which is a grade of service measure of the sent data, is the probability that the received signal strength falls below an information outage threshold ζ_I. It can be represented as a function of the end-to-end SNR γ_{E2E} at $\mathcal{D}$ as:

$$p_{out} = \Pr\left(\frac{1}{2}\log_2\left(1+\gamma_{E2E}\right) < \zeta_I\right). \quad (3)$$

The outage probability expressions in the two cases of $\mathcal{S}$-to-$\mathcal{D}$ reachability are obtained below.

1) No $\mathcal{S}$-to-$\mathcal{D}$ direct link available: Here, γ_{E2E} is bottlenecked by the weaker of the two SNRs: from $\mathcal{S}$-to-$\mathcal{R}$ and from $\mathcal{R}$-to-$\mathcal{D}$ [31]. Hence, outage probability, denoted as p_{out_1}, can be represented as a function of transmit powers (P_s, P_r) and the corresponding path losses as [32]:

$$\begin{aligned} p_{out_1} &= \Pr\left[\frac{1}{2}\log_2\left(1+\min\left\{\gamma_1,\rho\gamma_2\right\}\right) < \zeta_I\right] \\ &= \Pr\left[\min\left\{\gamma_1,\rho\gamma_2\right\} < 2^{2\zeta_I}-1\right] \\ &\overset{\mathcal{Z}\triangleq 2^{2\zeta_I}-1}{=} 1-\left(1-\Pr\left[\gamma_1<\mathcal{Z}\right]\right)\left(1-\Pr\left[\gamma_2<\frac{\mathcal{Z}}{\rho}\right]\right) \\ &= 1-\mathcal{C}_{\gamma_1}\left(\mathcal{Z}\right)\mathcal{C}_{\gamma_2}\left(\frac{\mathcal{Z}}{\rho}\right) \\ &\overset{\text{using (2)}}{=} 1-Q_1\left(\sqrt{2K_1},\sqrt{\frac{2(K_1+1)N_0 d^l \mathcal{Z}}{a_s P_s}}\right)\times \\ &\quad Q_1\left(\sqrt{2K_2},\sqrt{\frac{2(K_2+1)N_0\left(\frac{D}{\epsilon}-d\right)^l\mathcal{Z}}{\rho a_r P_r}}\right). \quad (4) \end{aligned}$$

To gain analytical insights on the performance of the proposed optimization schemes for SWIPT over Rician channels, we consider a recently developed tight exponential-type approximation [33] for $Q_1(\cdot,\cdot)$, which is being widely considered for Rician fading performance analysis [34]:

$$Q_1(a,b) \approx \exp\left(-e^{\phi(a)}b^{\varphi(a)}\right), \quad (5)$$

In above equation, the parameters $\phi(a)$ and $\varphi(a)$ are functions of a, and are given by:

$$\phi(a) = \begin{cases} \frac{45\pi^2+72\ln 2+20.7798-496}{64\left(9\pi^2-80\right)}a^4 - \frac{a^2}{2} - \ln 2, & a \ll 1 \\ -0.0045a^4 + 0.0858a^3 - 0.7529a^2 & \\ +0.3504a - 0.8526, & \text{otherwise,} \end{cases} \quad (6)$$

$$\text{and} \quad \varphi(a) = \begin{cases} \frac{9}{8\left(9\pi^2-80\right)}a^4 + 2, & a \ll 1 \\ 0.0053a^4 - 0.0910a^3 & \\ +0.5895a^2 - 0.5916a + 2.1793, & \text{otherwise.} \end{cases} \quad (7)$$

Employing the approximation (5) in (4) and using $P_r = P_T - P_s$, we obtain:

$$p_{out_1} \approx 1 - e^{-\left(\alpha_1\left(\frac{d^l}{a_s P_s}\right)^{\beta_1} + \alpha_2\left(\frac{(D-d)^l}{\rho a_r\left(P_T-P_s\right)}\right)^{\beta_2}\right)} \quad (8)$$

where $\alpha_i = e^{\phi\left(\sqrt{2K_i}\right)}\left(2(K_i+1)N_0\mathcal{Z}\right)^{\beta_i}$ and $\beta_i = \frac{\varphi\left(\sqrt{2K_i}\right)}{2}$ $\forall i \in \{0,1,2\}$ are positive functions of Rice factor K_i, noise power N_0, and outage threshold ζ_I (as $\mathcal{Z} \triangleq 2^{2\zeta_I}-1$). The accuracy of this exponential approximation has also been numerically verified in Section VIII-D.

2) $\mathcal{S}$-to-$\mathcal{D}$ direct link available: Here $\mathcal{D}$ combines the signals y_0 received from $\mathcal{S}$ in first slot and y_2 received from $\mathcal{R}$ in second slot using maximal ratio combining [7]. γ_{E2E} at $\mathcal{D}$ is:

$$\gamma_{E2E} = \min\left\{\gamma_1, \gamma_0 + \rho\gamma_2\right\} = \min\left\{\gamma_1, \Upsilon_{02}\right\} \quad (9)$$

where Υ_{02} is the effective SNR in the second slot which is the sum of positive weighted noncentral-χ^2 random variables. Although the distribution of this sum can be obtained in terms of Laguerre expansions [35], we consider its integral definition to avoid the unnecessary complications. Using (3) and (9), in

$$
\begin{aligned}
p_{out_2} &= \Pr\left[\min\left\{\gamma_1, \Upsilon_{02}\right\} < 2^{2\zeta_I} - 1\right] = 1 - \left(1 - \Pr\left[\gamma_1 < \mathcal{Z}\right]\right)\left(1 - \Pr\left[\Upsilon_{02} < \mathcal{Z}\right]\right) \\
&= 1 - \mathcal{C}_{\gamma_1}\left(\mathcal{Z}\right)\left(1 - \int_0^{\mathcal{Z}} \frac{\mathrm{d}F_{\gamma_0}\left(x\right)}{\mathrm{d}x} F_{\gamma_2}\left(\frac{\mathcal{Z}-x}{\rho}\right)\mathrm{d}x\right) \\
&\overset{\text{using (2),(5)}}{\approx} 1 - e^{-e^{\phi\left(\sqrt{2K_1}\right)}\left(\frac{2(K_1+1)N_0\mathcal{Z}d^l}{a_s P_s}\right)^{\beta_1}}\left[1 - \int_0^{\mathcal{Z}} \frac{\beta_0}{x}\left(\frac{2(K_0+1)N_0 x D^l}{a_d P_s}\right)^{\beta_0} e^{\phi\left(\sqrt{2K_0}\right)}\right. \\
&\quad \left. \times e^{-e^{\phi\left(\sqrt{2K_0}\right)}\left(\frac{2(K_0+1)N_0\mathcal{Z}D^l}{a_d P_s}\right)^{\beta_0}}\left(1 - e^{-e^{\phi\left(\sqrt{2K_2}\right)}\left(\frac{2(K_2+1)N_0(\mathcal{Z}-x)\left(\frac{D}{\epsilon}-d\right)^l}{\rho a_r\left(P_T - P_s\right)}\right)^{\beta_2}}\right)\mathrm{d}x\right].
\end{aligned} \tag{10}
$$

this case the outage probability, denoted by p_{out_2}, can be represented as a function of transmit powers $(P_s, P_r = P_T - P_s)$, $\mathcal{S}$-to-$\mathcal{R}$ distance d, and ρ as given in (10). Though the integral in (10) cannot be solved analytically, an efficient numerical solution can be easily obtained using commonly available commercial software, such as Matlab or Mathematica.

B. Optimization formulation

Given the outage probability p_{out} expressions (8) and (10) as functions of transmit powers (P_s, P_r), inter-nodal distances $(d, \frac{D}{\epsilon} - d)$, and PS ratio ρ, we are interested in finding optimal PA for $\mathcal{S}$ and $\mathcal{R}$, optimal RP between $\mathcal{S}$ and $\mathcal{D}$, and optimal ρ to minimize p_{out}, subject to harvested power constraint ($C1$), total power constraints ($C2$–$C3$), relay placement constraints ($C4$–$C5$), and normalization constraints on ρ ($C6$–$C7$). The optimization problem can be formulated as:

$$
\begin{aligned}
(\mathbf{J0}): \underset{P_s,d,\rho}{\text{minimize}}\ & p_{out} = \begin{cases} p_{out_1}, & \text{if } \mathcal{S}\text{-to-}\mathcal{D} \text{ direct link is not available} \\ p_{out_2}, & \text{if } \mathcal{S}\text{-to-}\mathcal{D} \text{ direct link is available} \end{cases} \\
\text{subject to}\quad & C1\text{: } P_{con}(P_s, d, \rho) \triangleq \zeta_P - \frac{\eta a_r (1-\rho)(P_T - P_s)}{\left(\frac{D}{\epsilon} - d\right)^l} \leq 0, \\
& C2: P_s \leq P_T, \qquad C3: P_s \geq 0, \qquad C4: d \leq \frac{D}{\epsilon} - \delta, \\
& C5: d \geq \delta, \qquad C6: \rho \leq 1, \qquad C7: \rho \geq 0.
\end{aligned} \tag{11}
$$

In (11), ζ_P is the minimum average harvested power required at $\mathcal{D}$ to have its continued operation. With normalized slot duration assumption, ζ_P is equivalent to the energy requirement at $\mathcal{D}$. In $C4$ and $C5$, $\delta = \frac{2fL^2}{c}$ is the minimum separation required between $\mathcal{S}$ and $\mathcal{R}$, or $\mathcal{R}$ and $\mathcal{D}$, for the antennas to be in far-field (Fraunhofer) region [27], where L is the largest dimension of the antenna structure, c is the speed of light, and f is the frequency of the transmitted signal.

1) Equivalence of exact and asymptotic p_{out_1} minimization problem: Minimizing the exponential approximation of exact outage probability p_{out_1} in (8) is equivalent to minimize its asymptotic (high SNR) version, denoted by $\widehat{p_{out_1}}$, obtained using $e^{-x} \approx 1 - x$, for $x \ll 1$,

$$
\widehat{p_{out_1}} = \alpha_1 \left(\frac{d^l}{a_s P_s}\right)^{\beta_1} + \alpha_2 \left(\frac{(D-d)^l}{\rho a_r \left(P_T - P_s\right)}\right)^{\beta_2}. \tag{12}
$$

The above observation holds because $p_{out_1} = 1 - e^{-\widehat{p_{out_1}}}$ is a strictly increasing function of $\widehat{p_{out_1}}$. As a result, the minimization problem with p_{out_1} as objective function is equivalent [36] to the one with $\widehat{p_{out_1}}$ as objective function, and both problems share the same set of optimal points (P_s^*, d^*, ρ^*). The optimal values, though different, are related as $p_{out_1}^* = 1 - e^{-\widehat{p_{out_1}}^*}$.

IV. Optimal Power Allocation for Fixed RP and PS ratio ρ

A. Optimal PA with no direct $\mathcal{S}$-to-$\mathcal{D}$ link available

Here we use the equivalence of exact and asymptotic p_{out_1} minimization for SWIPT without $\mathcal{S}$-to-$\mathcal{D}$ direct link (see Section III-B1) to obtain analytical expression for optimal PA. For a given ρ and RP d between $\mathcal{S}$ and $\mathcal{D}$, the problem of optimal PA for $\mathcal{S}$ and $\mathcal{R}$ that minimizes $\widehat{p_{out_1}}$ (or equivalently p_{out_1}), is obtained from (J0) with $\widehat{p_{out_1}}$ as objective function, P_s as optimization variable, and $C1$–$C3$ as constraints. Since $\mathcal{R}$ is placed on LOS path between $\mathcal{S}$ and $\mathcal{D}$, $\epsilon = 1$.

Associating the Lagrange multiplier λ with $C1$ and keeping the boundary constraints $C2$ and $C3$ ($0 \leq P_s \leq P_T$) implicit, the Lagrangian function of (PA1) is formulated as:

$$
\begin{aligned}
\mathcal{L}_1(P_s, d, \rho, \lambda) &= \alpha_1 \left(\frac{d^l}{a_s P_s}\right)^{\beta_1} + \alpha_2 \left(\frac{\left(\frac{D}{\epsilon} - d\right)^l}{\rho a_r \left(P_T - P_s\right)}\right)^{\beta_2} \\
&\quad + \lambda \left(\zeta_P - \frac{\eta a_r (1-\rho)(P_T - P_s)}{(\frac{D}{\epsilon} - d)^l}\right).
\end{aligned} \tag{13}
$$

As $\frac{\partial^2 \widehat{p_{out_1}}}{\partial P_s^2} = \frac{\alpha_1\beta_1(\beta_1+1)\left(\frac{d^l}{a_s P_s}\right)^{\beta_1} + \alpha_2\beta_2(\beta_2+1)P_s^2\left(\frac{(\frac{D}{\epsilon}-d)^l}{\mathrm{a}r\rho(P_T-P_s)}\right)^{\beta_2}}{P_s^2(P_T-P_s)^2}$ $> 0, \forall P_s \in [0, P_T]$ $\left(\text{and } 0 < d < \frac{D}{\epsilon}\right)$, $\widehat{p_{out_1}}$ is a strictly convex function of P_s in the feasible region defined by $C1$–$C3$. Since the constraints $C1$–$C3$ are affine functions of P_s, the global optimal solution for (PA1), denoted as P_s^*, is obtained using the Karush-Kuhn-Tucker (KKT) conditions [37] given by: $C1$–$C3$, $\lambda \geq 0$,

$$
\frac{\partial \mathcal{L}_1}{\partial P_s} = \frac{\alpha_2\beta_2(\frac{D}{\epsilon} - d)^{\beta_2 l}}{(\rho a_r)^{\beta_2}\left(P_T - P_s\right)^{\beta_2+1}} - \frac{\alpha_1\beta_1 d^{\beta_1}}{a_s^{\beta_1} P_s^{\beta_1+1}} + \lambda \frac{\eta a_r (1-\rho)}{\left(\frac{D}{\epsilon} - d\right)^l} = 0, \tag{14a}
$$

$$
\text{and}\quad \lambda \left(\zeta_P - \frac{\eta a_r (1-\rho)(P_T - P_s)}{(\frac{D}{\epsilon} - d)^l}\right) = 0. \tag{14b}
$$

If $P_s^* = P_T$, $C1$ cannot be satisfied $\forall\ \zeta_P > 0$. Thus, $P_s^* < P_T$. If $\lambda^* \neq 0$, then

$$
P_s^* = P_s^{th} \triangleq P_T - \frac{\zeta_P \left(\frac{D}{\epsilon} - d\right)^l}{\eta a_r (1-\rho)} \tag{15}
$$

$$\lambda_{P_s}^{th}=\frac{\alpha_1\beta_1\rho^{\beta_2}\zeta_P^{\beta_2+1}\left[a_r\eta\left(1-\rho\right)d^l\right]^{\beta_1}\left(\frac{D}{\epsilon}-d\right)^l-\alpha_2\beta_2 a_s^{\beta_1}\left[\eta a_r P_{_T}(1-\rho)-\zeta_P\left(\frac{D}{\epsilon}-d\right)^l\right]^{\beta_1+1}\left[\eta(1-\rho)\right]^{\beta_2}}{a_s^{\beta_1}\rho^{\beta_2}\zeta_P^{\beta_1+1}\left[\left(\eta a_r P_{_T}(1-\rho)-\zeta_P\left(\frac{D}{\epsilon}-d\right)^l\right)\right]^{\beta+1}}. \quad (16)$$

so that (14b) is satisfied. Using (14a), $\lambda^*=\lambda_{P_s}^{th}$ for $P_s^*=P_s^{th}$ is given by (16).

Here, P_s^{th} is the maximum threshold power that can be allocated to $\mathcal{S}$ so that PA to $\mathcal{R}$, $P_r^*=P_{_T}-P_s^{th}$ satisfies $C1$. *As P_s^{th} is a decreasing function of ζ_P, PA to $\mathcal{S}$ decreases with increasing ζ_P and more power is allocated to $\mathcal{R}$ to meet $C1$ (harvested power constraint), which leads to increasing p_{out_1} due to weakening of $\mathcal{S}$-to-$\mathcal{R}$ link.* However, if $P_s^{th}<0$, then (PA1) is infeasible, as $C1$ is never satisfied. Mathematically, $P_s^*=0$ is a feasible solution, though it gives $p_{out_1}=1$.

If $P_s^*<P_s^{th}$, then $\lambda^*=0$ to satisfy (14b), which on substitution in (14a) gives:

$$\frac{\left(P_{_T}-P_s\right)^{\beta_2+1}}{P_s^{\beta_1+1}}=\frac{\alpha_2\beta_2}{\alpha_1\beta_1}\left(\frac{a_s}{d^l}\right)^{\beta_1}\left(\frac{(D-d)^l}{\rho a_r}\right)^{\beta_2}. \quad (17)$$

P_s^* for $\lambda^*=0$, denoted by $P_{s_1}^0$, can be obtained by using the standard root-finding algorithms to find the efficient numerical solution of (17). However, for the same Rice factor, i.e., $K\triangleq K_1=K_2$, which implies $\alpha_1=\alpha_2$ and $\beta_1=\beta_2$, analytical closed form solution of (17) is given by: $P_s^*=P_{s_1}^0\triangleq\frac{P_{_T}\left(a_r\rho\left(\frac{d}{D-d}\right)^l\right)^{\frac{\beta_1}{\beta_1+1}}}{a_s^{\frac{\beta_1}{\beta_1+1}}+\left(a_r\rho\left(\frac{d}{D-d}\right)^l\right)^{\frac{\beta_1}{\beta_1+1}}}$. *From the expression of $P_{s_1}^0$ it is clear that optimal PA is such that higher power is allocated to $\mathcal{S}$, if $\mathcal{R}$ is closer to $\mathcal{D}$.* It may be noted that, under the condition $P_{s_1}^0\leq P_s^{th}$, we have the special case where the expression for $P_{s_1}^0$, which is independent of ζ_P, is similar to the ones obtained in [2]–[4]. This is because, the condition $P_{s_1}^0\leq P_s^{th}$ arises when ζ_P is very low and the harvested power constraint $C1$ is implicitly satisfied, thereby reducing the PA optimization solely to make information transfer efficient, i.e., only to minimize p_{out_1}. However, if ζ_P is increased, P_s^{th} decreases, and once it drops below $P_{s_1}^0$, the role of harvested power constraint becomes significant which influences the minimum p_{out_1}. It follows that there exists a tradeoff between minimized p_{out_1} and the lower bound ζ_P on required harvested power at $\mathcal{D}$ for $P_{s_1}^0>P_s^{th}$. Hence, the optimal solution of (PA1) is given by:

$$(P_s^*,\lambda^*)=\begin{cases}\left(P_{s_1}^0,0\right), & P_{s_1}^0\leq P_s^{th}\\ \left(P_s^{th},\lambda_{P_s}^{th}\right), & 0\leq P_s^{th}<P_{s_1}^0\\ \text{Infeasible}, & P_s^{th}<0.\end{cases} \quad (18)$$

For $P_s^{th}<P_{s_1}^0$, $P_{_T}<\frac{\zeta_P(D-d)^l}{\eta a_r(1-\rho)}\left[1+\left(\frac{a_r\rho\left(\frac{d}{D-d}\right)^l}{a_s}\right)^{\frac{\beta_1}{\beta_1+1}}\right]$, which after some simplification gives:

$$\zeta_P\left[a_r\rho d^l\left(D-d\right)^l\right]^{\frac{\beta_1}{\beta_1+1}}>a_s^{\frac{\beta_1}{\beta_1+1}}\left[\eta a_r P_{_T}(1-\rho)-\zeta_P\left(D-d\right)^l\right]. \quad (19)$$

From (16) and (19), $\lambda_{P_s}^{th}>0\;\forall\;P_s^{th}$, subject to $0\leq P_s^{th}<P_{s_1}^0$.

B. Optimal PA with direct $\mathcal{S}$-to-$\mathcal{D}$ link available

For a fixed RP and ρ, the problem of optimal PA at $\mathcal{S}$ and $\mathcal{R}$ with direct $\mathcal{S}$-to-$\mathcal{D}$ link available, denoted by (PA2) is similar to (PA1), but with p_{out_2} being the objective function to be minimized. From (10), p_{out_2} is a nonconvex function of P_s. In this regard, we first define pseudoconvex function [37] and then claim that p_{out_2} is a pseudoconvex function of P_s satisfying $C1$–$C3$.

Definition 1: A differentiable function $f\colon\mathbb{R}^n\to\mathbb{R}$, defined on a nonempty open convex set Ω, is called pseudoconvex if $\forall\;x,y\in\Omega$ with $x\neq y$, $\nabla f\left(x\right)^{\mathsf{T}}\left(y-x\right)\geq 0\implies f(y)\geq f(x)$. A pesudoconvex function f has a similar property as in convex functions, which states that, if $\exists$ a critical point, i.e., $\nabla f(\overline{x})=0$, then $\overline{x}$ is a global minimum [36].

Lemma 1: p_{out_2} is a pseudoconvex function of $P_s\in\{P_s\mid(P_{con}\left(P_s,d,\rho\right)\leq P_{_T})\wedge(0\leq P_s\leq P_{_T})\}$.

Proof: See Appendix A-A. ∎

To find the global optimal PA $(P_s^*,P_r^*=P_{_T}-P_s^*)$ for a fixed RP and ρ problem (PA2), while accounting the harvested power constraint ($C1$) and the total power constraints ($C2$ and $C3$), we use the convexity of $C1$–$C3$, along with the proposed Lemma 1 and the following lemma.

Lemma 2 ([36, Theorem 4.3.8]): Consider a constraint minimization problem (*CMP*) with an objective function to be minimized over a feasible region S being pseudoconvex at $\overline{x}\in S$, constraint functions are differentiable and quasiconvex at $\overline{x}$, and the KKT conditions hold at $\overline{x}$. Then $\overline{x}$ is a global optimal solution to *CMP*.

Associating the Lagrange multiplier μ with the harvested power constraint $C1$ and keeping the boundary constraints $C2$–$C3$ implicit, Lagrangian function of (PA2) is given by:

$$\mathcal{L}_2(P_s,d,\rho,\mu)=p_{out_2}+\mu\left(\zeta_P-\frac{\eta a_r(1-\rho)(P_{_T}-P_s)}{\left(\frac{D}{\epsilon}-d\right)^l}\right). \quad (20)$$

Following Lemma 2 and (20), we next define the KKT conditions (stationarity and complimentary slackness only, as the primal and dual feasibility conditions are given by $C1$–$C3$ and $\mu\geq 0$):

$$\frac{\partial\mathcal{L}_2}{\partial P_s}=\frac{\partial p_{out_2}}{\partial P_s}+\mu\left(\frac{\eta a_r(1-\rho)}{\left(\frac{D}{\epsilon}-d\right)^l}\right)=0 \quad (21)$$

$$\mu\left(\zeta_P-\frac{\eta a_r(1-\rho)(P_{_T}-P_s)}{\left(\frac{D}{\epsilon}-d\right)^l}\right)=0. \quad (22)$$

With $P_s^*=P_{_T}$, $C1$ cannot be satisfied $\forall\;\zeta_P>0$. Thus, $P_s^*<P_{_T}$. If $\mu^*\neq 0$, then $P_s^*=P_s^{th}$, as defined in (15) so that (22) is satisfied. $\mu^*=\mu_{P_s}^{th}>0$ for $P_s^*=P_s^{th}$ can be obtained using the value of derivative of (10) with respect to P_s at P_s^{th} $\left(\text{i.e., }\nabla_{_{P_s}}\;p_{out_2}\left(P_s^{th}\right)\right)$ and (21) as:

$$\mu_{P_s}^{th}=-\frac{\left[\nabla_{_{P_s}}\;p_{out_2}\left(P_s^{th}\right)\right]\left(\frac{D}{\epsilon}-d\right)^l}{\eta a_r(1-\rho)}. \quad (23)$$

Similar to (PA1), if $P_s^{th} < 0$, then (PA2) is infeasible, as $C1$ is never satisfied. $P_s^* = 0$ is a feasible solution, though it gives $p_{out_2} = 1$. If $\mu^* = 0$, then $P_s^* < P_s^{th}$; (22) is satisfied and (21) implies finding the critical point of $p_{out_2}(P_s)$. From (10) and the discussion in Section III-A2, it can be observed that, due to the presence of highly non-linear terms in p_{out_2}, it is not possible to obtain the explicit analytic solution for (21) in P_s with $\mu = 0$. Thus, we use the Conjugate Gradient Method (CGM) with positive Polak-Ribiere (PR) beta [38] to find the global optimal solution P_s^* for (PA2) by numerically solving $\frac{\partial p_{out_2}}{\partial P_s} = 0$, if the critical point exists. Let us denote the global optimal PA P_s^* returned by the CGM algorithm by $P_{s_2}^0$. We also use Golden-section (GS) based linear search [39] technique to restrict the search in CGM within the upper and lower bounds $(0 \leq P_s \leq P_T)$ such that feasibility constraints are met. Note that, this iterative algorithm provides very good convergence due to the pseudoconvexity of the problem.

$P_{s_2}^0$ is independent of ζ_P and, since for $P_{s_2}^0 < P_s^{th}$, $C1$ is not active, it implies that $P_s^* = P_{s_2}^0$ provides the minimum p_{out_2} for a predetermined RP and ρ. Similar to (PA1), a tradeoff between minimized p_{out_2} and ζ_P exists for $P_{s_2}^0 > P_s^{th}$. The optimal solution is given by:

$$(P_s^*, \mu^*) = \begin{cases} \left(P_{s_2}^0, 0\right), & P_{s_2}^0 \leq P_s^{th} \\ \left(P_s^{th}, \mu_{P_s}^{th}\right), & 0 \leq P_s^{th} < P_{s_2}^0 \\ \text{Infeasible}, & P_s^{th} < 0. \end{cases} \tag{24}$$

V. Optimal Relay Placement for Fixed PA and PS ratio ρ

A. Optimal RP with no direct $\mathcal{S}$-to-$\mathcal{D}$ link available

For a predetermined PA (P_s, P_r) and ρ, we now obtain optimal RP, i.e., distance d^* between $\mathcal{S}$ and $\mathcal{R}$, or $(D - d^*)$ between $\mathcal{R}$ and $\mathcal{D}$, with $\mathcal{R}$ placed on the direct $\mathcal{S}$-to-$\mathcal{D}$ path (Fig. 1(a)). The problem of optimal RP $(d^*, D - d^*)$, denoted as (RP1), can be obtained from (11), with $\widehat{p_{out_1}}$ as objective function to be minimized over the variable d subject to constraints $C1$, $C4$–$C5$.

As $\frac{\partial^2 \widehat{p_{out_1}}}{\partial d^2} = \frac{\alpha_1\beta_1 l(\beta_1 l - 1) d^{\beta_1 l - 2}}{(a_s P_s)^{\beta_1}} + \frac{\alpha_2\beta_2 l(\beta_2 l - 1)\left(\frac{D}{\epsilon} - d\right)^{\beta_2 l - 2}}{\left(a_r \rho \left(P_T - P_s\right)\right)^{\beta_2}} > 0, \forall d \in \left[\delta, \frac{D}{\epsilon} - \delta\right]$ $\left(\text{and } (l > 1) \wedge (P_s \in [0, P_T])\right)$, $\widehat{p_{out_1}}$ is a strictly convex function of d in the feasible region defined by $C1$, $C4$–$C5$. Since $C1, C4$–$C5$ are convex functions of d, the global solution for (RP1), d^*, can be obtained using the KKT conditions given by (25), (14b), along with $C1$, $C4$–$C5$, and $\lambda \geq 0$.

$$\begin{aligned} \frac{\partial \mathcal{L}_1}{\partial d} &= \frac{\alpha_1\beta_1 l d^{\beta_1 l - 1}}{(a_s P_s)^{\beta_1}} - \frac{\alpha_2\beta_2 l\left(\frac{D}{\epsilon} - d\right)^{\beta_2 l - 1}}{\left[\rho a_r \left(P_T - P_s\right)\right]^{\beta_2}} \\ &\quad + \lambda\left(-\frac{\eta a_r l(1-\rho)(P_T - P_s)}{\left(\frac{D}{\epsilon} - d\right)^{l+1}}\right) = 0. \end{aligned} \tag{25}$$

If $\lambda^* \neq 0$, $d^* = d^{th}$ that satisfies (14b) is defined as follows:

$$d^* = d^{th} \triangleq \frac{D}{\epsilon} - \left(\frac{\eta a_r (1-\rho)(P_T - P_s)}{\zeta_P}\right)^{1/l}. \tag{26}$$

Using (25), for $d^* = d^{th}$, $\lambda^* = \lambda_d^{th}$ is given by (27). *Note that, d^{th} is the minimum threshold distance of $\mathcal{R}$ from $\mathcal{S}$, such that the received power P_r at $\mathcal{D}$ satisfies C1. d^{th} is an increasing function of ζ_P and, if $d^{th} > \frac{D}{\epsilon} - \delta$, then (RP2) is infeasible.*

If $d^* > d^{th}$, then $\lambda^* = 0$, which, by using (25) gives,

$$\frac{d^{\beta_1 l - 1}}{(D - d)^{\beta_2 l + 1}} = \frac{\alpha_2\beta_2 \left(a_s P_s\right)^{\beta_1}}{\alpha_1\beta_1 \left(\rho a_r \left(P_T - P_s\right)\right)^{\beta_2}}. \tag{28}$$

Although closed-form analytical solution cannot be obtained for (28), an efficient numerical solution, denoted by d_1^0, can be obtained using easily available standard root-finding algorithms. If we again consider same Rice factor for all the links, i.e., $\alpha_1 = \alpha_2$ and $\beta_1 = \beta_2$, analytical closed form solution of (28) is given by: $d^* = d_1^0 \triangleq \max\left[\delta, \min\left\{\frac{D(a_s P_s)^{\frac{\beta_1}{\beta_1 l - 1}}}{\left[a_r \rho (P_T - P_s)\right]^{\frac{\beta_1}{\beta_1 l - 1}} + (a_s P_s)^{\frac{\beta_1}{\beta_1 l - 1}}}, D - \delta\right\}\right]$, so that d_1^0 does not violate upper and lower bounds on d. Optimal solution of (RP1) is given by:

$$(d^*, \lambda^*) = \begin{cases} \left(d_1^0, 0\right), & d_1^0 \geq d^{th} \\ \left(d^{th}, \lambda_d^{th}\right), & d_1^0 < d^{th} \leq D - \delta \\ \text{Infeasible}, & d^{th} > D - \delta. \end{cases} \tag{29}$$

Note that, (29) gives the feasible region for (RP1) if $P_s < P_T$ (or $P_r > 0$). If $d^{th} > d_1^0$, then $D > \left(\frac{\eta a_r (1-\rho)(P_T - P_s)}{\zeta_P}\right)^{\frac{1}{l}} \left[1 + \left(\frac{a_s P_s}{a_r \rho (P_T - P_s)}\right)^{\frac{\beta_1}{\beta_1 l - 1}}\right]$, which after some rearrangement gives:

$$d^{th}[a_r \rho (P_T - P_s)]^{\frac{\beta_1}{\beta_1 l - 1}} > \left(D - d^{th}\right)(a_s P_s)^{\frac{\beta_1}{\beta_1 l - 1}}. \tag{30}$$

From (27) and (30), $\lambda_d^{th} > 0 \ \forall \ d^{th}$, with $d_1^0 < d^{th} \leq D - \delta$. Similar to as noted in Section IV-A, with $d_1^0 \geq d^{th}$, we have a special case where the expression for d_1^0 is similar to the ones obtained in [2]–[4]. This is because, the condition $d_1^0 \geq d^{th}$ arises when ζ_P is very low and $C1$ is implicitly met, so optimal RP is carried out solely to minimize p_{out_1}. Also, optimal RP in this case, $d^* = d_1^0$, is such that for higher PA to $\mathcal{S}$, $\mathcal{R}$ is placed closer to $\mathcal{D}$. But, as ζ_P is increased depending on the energy requirements at $\mathcal{D}$, d^{th} increases. If $d^{th} > d_1^0$, then optimal RP $d^* = d^{th}$, is dependent on ζ_P, and thus there exists a tradeoff between the minimized p_{out_1} and ζ_P.

B. Optimal RP with $\mathcal{S}$-to-$\mathcal{D}$ direct link available

For a predetermined PA $(P_s,\ P_r)$ and ρ, the optimal RP problem (RP2) of finding the optimal distance distance d^* between $\mathcal{S}$ and $\mathcal{R}$, or $\left(\frac{D}{\epsilon} - d^*\right)$ between $\mathcal{R}$ and $\mathcal{D}$, with $\mathcal{R}$ placed on the elliptical path with $\mathcal{S}$ and $\mathcal{D}$ as the *foci* (see Fig. 1(b)) that minimizes p_{out_2}, has same optimization variable and constraints as (RP1), except the objective function to be minimized being p_{out_2}.

The constraint function defined in $C1$ is convex in d, and $C4$ and $C5$ are affine functions of d. In the following lemma, we claim that p_{out_2} is pseudoconvex in d in the feasible RP region $\mathcal{F}_d = \left\{d \mid \left(P_{con}\left(P_s, d, \rho\right) \leq 0\right) \wedge \left(\delta \leq d \leq \frac{D}{\epsilon} - \delta\right)\right\}$ as defined by the constraints $C1$, $C4$, and $C5$.

Lemma 3: Outage probability p_{out_2} is a pseudoconvex function of $\mathcal{S}$-to-$\mathcal{R}$ distance $d \in \mathcal{F}_d$.

Proof: See Appendix B-A. ∎

The pseudoconvexity of p_{out_2} in d is due to the log-concavity of complimentary CDFs of γ_1 and Υ_{02}, i.e., $\mathcal{C}_{\gamma_1}$ and $\mathcal{C}_{\Upsilon_{02}}$, respectively, in $\mathcal{S}$-to-$\mathcal{R}$ distance d (see Appendix B for details).

$$\lambda_d^{th}=\frac{\alpha_1\beta_1\left(D-d^{th}\right)\left(d^{th}\right)^{\beta_1 l}\left(a_r\rho\left(P_{_T}-P_s\right)\right)^{\beta_2}-\alpha_2\beta_2\left(a_sP_s\right)^{\beta_1}d^{th}\left(D-d^{th}\right)^{\beta_2 l}}{\eta\left(1-\rho\right)\left(a_sP_s\right)^{\beta_1}\left(a_r\left(P_{_T}-P_s\right)\right)^{\beta_2+1}d^{th}\left[\left(D-d^{th}\right)^{l}\right]^{-1}}. \tag{27}$$

The KKT conditions for (RP2) are given by (31) and (22), along with $C1$, $C4$–$C5$, and $\mu \geq 0$.

$$\frac{\partial\mathcal{L}_2}{\partial d}=\frac{\partial p_{out_2}}{\partial d}+\mu\left(-\frac{\eta a_r l(1-\rho)(P_{_T}-P_s)}{\left(\frac{D}{\epsilon}-d\right)^{l+1}}\right)=0. \tag{31}$$

If $\mu^*>0, d^*=d^{th}$ as defined in (26) with $\epsilon<1$, so that $C1$ and (14b) are satisfied. The value of $\mu^*=\mu_d^{th}$ at $d^*=d^{th}$ is obtained using $\nabla_d\, p_{out_2}\left(d^{th}\right)$ and (31) as:

$$\mu_d^{th}=\frac{\left[\nabla_d\, p_{out_2}\left(d^{th}\right)\right]\left(\frac{D}{\epsilon}-d\right)^{l+1}}{\eta a_r l(1-\rho)(P_{_T}-P_s)}. \tag{32}$$

If $\mu^*=0$, then $d^*>d^{th}$; (22) is satisfied and (31) implies finding the critical point of p_{out_2}, i.e., $\frac{\partial p_{out_2}}{\partial d}=0$. Observe from (10) that similar to p_{out_2}, $\frac{\partial p_{out_2}}{\partial d}$ contains highly non-linear terms. Therefore, it is not possible to obtain the explicit analytic solution of (31) for d^* with $\mu=0$. Again, we use CGM with positive PR beta and GS based linear search techniques to find d^* for (RP2) by indirectly solving $\frac{\partial p_{out_2}}{\partial d}=0$ (if the critical point exists), while restricting the search within the upper and lower bounds $\left(\delta\leq d\leq\frac{D}{\epsilon}-\delta\right)$. We denote the global optimal PA d^* obtained from CGM algorithm by d_2^0. So, optimal solution of (RP2) is given by:

$$(d^*,\mu^*)=\begin{cases}\left(d_2^0,0\right), & d_2^0\geq d^{th}\\ \left(d^{th},\mu_d^{th}\right), & d_2^0<d^{th}\leq\frac{D}{\epsilon}-\delta\\ \text{Infeasible}, & d^{th}>\frac{D}{\epsilon}-\delta.\end{cases} \tag{33}$$

Thus, (33) gives the feasible region for (RP2) if $P_s<P_{_T}$ (i.e., some power is allocated to $\mathcal{R}$). Also, $\mu_d^{th}>0\ \forall\ d^{th}$, with $d_2^0<d^{th}\leq\frac{D}{\epsilon}-\delta$. d_2^0, independent of ζ_P, corresponds to the case when $C1$ is not active, thus providing the minimum outage probability for a predetermined PA and ρ. Similar to as noted in Section V-A, with increased energy requirement ζ_P at $\mathcal{D}$, d^{th} increases and, if $d_2^0<d^{th}\leq\frac{D}{\epsilon}-\delta$, then there exists a tradeoff between minimized p_{out_2} and ζ_P.

VI. Optimal PS Ratio ρ For Fixed PA and RP

In this section we derive optimal PS for a predetermined PA and RP. The optimization problem in this case, denoted as (PS0), is formulated using (11) with ρ as the optimization variable and $C1$, $C6$–$C7$ as the constraints. Due to the monotonicity of outage probability in ρ, we consider the same optimization problem (PS0) for both with and without direct $\mathcal{S}$-to-$\mathcal{D}$ link cases. As ρ is the ratio of total power received at $\mathcal{D}$, which is utilized for information decoding, higher ρ gives lesser $p_{out_i}\forall i=1,2$. Next we discuss convexity of (PS0) and then obtain optimal ρ^*.

A. Convexity of $\widehat{p_{out_1}}$ in ρ

As $\frac{\partial^2\widehat{p_{out_1}}}{\partial\rho^2}=\frac{\alpha_2\beta_2(\beta_2+1)}{\rho^2}\left(\frac{(D-d)^l}{\rho a_r\left(P_{_T}-P_s\right)}\right)^{\beta_2}>0,\forall\rho\in[0,1]$ (and $0<P_s<P_{_T}$, $\delta<d<D-\delta$), $\widehat{p_{out_1}}$ is a strictly convex function of ρ in the feasible region defined by $C1$, $C6$–$C7$. Since the constraints $C1, C6$–$C7$ are linear functions of ρ, and the gradient of $\widehat{p_{out_1}}$ does not vanish in the feasible region, the global solution for (PS0), ρ^*, is given by the corner point obtained by solving $C1$ at strict equality, i.e., $\rho^*=\rho^{th}\triangleq 1-\frac{\zeta_P\left(\frac{D}{\epsilon}-d\right)^l}{\eta a_r\left(P_{_T}-P_s\right)}$. Here ρ^{th} is the maximum portion of the average received power at $\mathcal{D}$ that can be allocated for information decoding while satisfying $C1$. With $\mathcal{L}_1$ as the Lagrangian function for (PS0), the Lagrange multiplier λ_ρ^{th} in this case is:

$$\lambda_\rho^{th}=\frac{1}{\eta}\left(\frac{(D-d)^l}{a_r\rho\left(P_{_T}-P_s\right)}\right)^{\beta_2+1}>0\ \forall\left\{(d\leq D)\wedge(P_s\leq P_{_T})\right\}. \tag{34}$$

B. Pseudoconvexity of p_{out_2} in ρ

Lemma 4: Outage probability p_{out_2} is a pseudoconvex function of $\rho\in\mathcal{F}_{_\rho}=\{\rho\mid 0\leq\rho\leq 1\}$.

Proof: See Appendix C. ∎

So, using Lemma 2 and Lemma 4, the KKT point of (PS0) provides the global optimal solution. However, like in Section VI-A, here also the KKT point is obtained by solving $C1$ for ρ at strict equality, which gives $\rho^*=\rho^{th}$. The Lagrange multiplier μ_ρ^{th}, obtained by solving $\frac{\partial\mathcal{L}_2}{\partial\rho}=0$, is:

$$\mu_\rho^{th}=-\frac{\left[\nabla_\rho\ p_{out_2}\left(\rho^{th}\right)\right]\left(\frac{D}{\epsilon}-d\right)^l}{\eta a_r\left(P_{_T}-P_s\right)}>0,\ \text{because}\ \nabla_\rho p_{out_2}\left(\rho^{th}\right)<0. \tag{35}$$

It may be noted that PS optimization has least complexity in terms of implementation, among the three proposed semi-adaptive schemes. The optimal solution of (PS0) is given by:

$$(\rho^*,\lambda^*)=\begin{cases}\left(\rho^{th},\lambda_\rho^{th}\right), & \rho^{th}\geq 0\text{ with no direct }\mathcal{S}\text{-to-}\mathcal{D}\text{ link},\\ \left(\rho^{th},\mu_\rho^{th}\right), & \rho^{th}\geq 0\text{ with direct link availability},\\ \text{Infeasible}, & \rho^{th}<0.\end{cases} \tag{36}$$

VII. Joint Optimization of PA, RP, and ρ to Minimze Outage Probability

Here we derive the joint-optimal solutions with and without $\mathcal{S}$-to-$\mathcal{D}$ direct link.

A. Joint optimization with no direct $\mathcal{S}$-to-$\mathcal{D}$ link available

As noted in Section VI, outage probability is a strictly decreasing function of ρ, which implies that $C1$ in joint optimization problem should be satisfied with strict equality. This reduces three-variable minimization problem (J0) for p_{out_1} in (8) into an equivalent two-variable problem (J1).

$$\begin{aligned}(\mathbf{J1}):\ \underset{P_s,d}{\text{minimize}}\quad & \widehat{p_{out_1J}}\triangleq\alpha_1\left(\frac{d^l}{a_sP_s}\right)^{\beta_1}+\\ & \alpha_2\left(\frac{\eta\left(D-d\right)^l}{\eta a_r\left(P_{_T}-P_s\right)-\zeta_P\left(D-d\right)^l}\right)^{\beta_2}\\ \text{subject to}\quad & C2,C3,C4,C5,\ \text{and}\\ & C8: g_{C8}\triangleq\frac{\zeta_P\left(\frac{D}{\epsilon}-d\right)^l}{\eta a_r\left(P_{_T}-P_s\right)}-1\leq 0.\end{aligned} \tag{37}$$

Theorem 1: Outage probability $\widehat{p_{out_{1J}}}$ is a convex function of source power P_s and $\mathcal{S}$-to-$\mathcal{R}$ distance d over feasible region defined by the convex constraints $C2$–$C5$ and $C8$. So, the KKT point yields the global optimal solution of (J1).

Proof: The joint convexity of $\widehat{p_{out_{1J}}}$ is proved in Appendix D. $C2$–$C5$ are affine functions of P_s and d. Whereas, $C8$ is a convex function of P_s and d (see Appendix E). Using these results, along with Lemma 2, proves that KKT point is the global optimal solution of (J1). ∎

It may be noted that the constraint $C8$ along with $C2$–$C3$ provide upper and lower bounds on P_s, given as: $0 \leq P_s \leq \max\left\{0, P_T - \frac{\zeta_P (D-d)^l}{\eta a_r}\right\}$. Similarly, bounds on d, obtained using $C4$–$C5$ and $C8$, are given as $\max\left\{\delta, D - \left(\frac{\eta a_r \left(P_T - P_s\right)}{\zeta_P}\right)^{\frac{1}{l}}\right\} \leq d \leq D - \delta$. Keeping these boundary constraints implicit, (J1) can be solved as an unconstrained problem, whose Lagrangian function is given by $\widehat{p_{out_{1J}}}$ itself. So, the stationarity KKT conditions for (J1) are given by:

$$\frac{\partial \widehat{p_{out_{1J}}}}{\partial P_s} = \frac{\alpha_2 \beta_2 \eta^{\beta_2+1} a_r \left(D-d\right)^{\beta_2 l}}{\left(\eta a_r \left(P_T - P_s\right) - \zeta_P \left(D-d\right)^l\right)^{\beta_2+1}} - \frac{\alpha_1 \beta_1 d^{\beta_1 l}}{a_s^{\beta_1} P_s^{\beta_1+1}} = 0, \tag{38a}$$

$$\frac{\partial \widehat{p_{out_{1J}}}}{\partial d} = \frac{\alpha_1 \beta_1 l d^{\beta_1 l-1}}{\left(a_s P_s\right)^{\beta_1}} - \frac{\alpha_2 \beta_2 \eta^{\beta_2+1} a_r \left(P_T - P_s\right) l \left(D-d\right)^{\beta_2 l-1}}{\left(\eta a_r \left(P_T - P_s\right) - \zeta_P \left(D-d\right)^l\right)^{\beta_2+1}} = 0. \tag{38b}$$

On solving (38a) and (38b) for $P_s = P_s^J$ and $d = d^J$ with $\alpha_1 = \alpha_2$, $\beta_1 = \beta_2$, we obtain $d^J \triangleq D \frac{P_s^J}{P_T}$, where P_s^J is obtained by finding the root of (39) in interval $\left[\max\left\{0, P_T - \left[\left(\frac{P_T}{D}\right)^l \frac{a_r \eta}{\zeta_P}\right]^{\frac{1}{l-1}}\right\}, P_T\right]$.

$$\frac{\alpha_2 \beta_2 \eta^{\beta_2+1} D^{\beta_2 l} a_r P_T^l \left(P_T - P_s^J\right)^{\beta_2(l-1)-1}}{\left(\eta a_r P_T^l - \zeta_P D^l \left(P_T - P_s^J\right)^{l-1}\right)^{\beta_2+1}} = \left(\frac{D}{P_T}\right)^{\beta_1 l} \frac{\alpha_1 \beta_1 \left(P_s^J\right)^{\beta_1(l-1)-1}}{a_s^{\beta_1}}. \tag{39}$$

So, $d^* = \max\left[\delta, \min\left\{d^J, D-\delta\right\}\right]$, using which P_s^* is obtained as,

$$P_s^* = \begin{cases} \frac{\left(\frac{(d^*)^{\beta_1 l}}{a_r a_s^{\beta_1} \eta^{\beta_1+1} (D-d^*)^{\beta_1 l}}\right)^{\frac{1}{\beta_1+1}} \left(\eta a_r p_T - \zeta_P (D-d^*)^l\right)}{1+\eta a_r \left(\frac{(d^*)^{\beta_1 l}}{a_r a_s^{\beta_1} \eta^{\beta_1+1} (D-d^*)^{\beta_1 l}}\right)^{\frac{1}{\beta_1+1}}}, & ((d^* = \delta) \vee (d^* = D-\delta)) \\ P_s^J, & \delta < d^* < D-\delta. \end{cases} \tag{40}$$

Following this, $\rho^* = 1 - \frac{\zeta_P (D-d^*)^l}{\eta a_r \left(P_T - P_s^*\right)}$. *So, (P_s^*, d^*, ρ^*) is the joint-optimal solution of (J1) if $\zeta_P \leq \frac{\eta a_r P_T}{\delta^l}$; otherwise the problem is infeasible.* As P_s^*, d^*, and ρ^* are all functions of ζ_P, there exists a tradeoff between minimized p_{out_1} and ζ_P. Minimized p_{out_1} obtained from the joint optimization is better (lower) than the three partially-adaptive optimization schemes (only PA, or only RP, or only PS), as shown via numerical results in Section VIII-E. Indeed, besides utilizing the optimal amount of received energy for harvesting, simultaneously $\mathcal{R}$ can be moved closer to $\mathcal{D}$ and the weaker $\mathcal{S}$-to-$\mathcal{R}$ link can be improved by allocating a higher power to $\mathcal{S}$.

B. Joint optimization with $\mathcal{S}$-to-$\mathcal{D}$ direct link available

Using the problem definitions for (J0) and (J1) provided in Sections III-B and VII-A, respectively, an equivalent two-variable joint optimization problem that minimizes p_{out_2} is given as:

$$(\mathbf{J2}): \underset{P_s, d}{\text{minimize}} \quad p_{out_{2J}}, \quad \text{subject to} \quad C2, C3, C4, C5, C8. \tag{41}$$

Here, $p_{out_{2J}}$, obtained by substituting $\rho = 1 - \frac{\zeta_P \left(\frac{D}{\epsilon} - d\right)^l}{\eta a_r \left(P_T - P_s\right)}$ in (10), is jointly nonconvex in P_s and d. In this regard, we first define a bi-pseudoconvex function and then we use it in Theorem 2.

Definition 2: A function $f(x, y)$ with $x \in X$ and $y \in Y$, defined over a bi-convex set $B \subset X \times Y$, is called a bi-pseudoconvex if upon fixing $x = \overline{x}$, $f_x(y) = f(\overline{x}, y)$ is pseudoconvex over Y, and fixing $y = \overline{y}$, $f_y(x) = f(x, \overline{y})$ is pseudoconvex over X.

Theorem 2: Outage probability $p_{out_{2J}}$ is a bi-pseudoconvex function of source power P_s and $\mathcal{S}$-to-$\mathcal{R}$ distance d over the bi-convex set B' defined by the constraints $C2$–$C5$ and $C8$.

Proof: Outage probability $p_{out_{2J}}$: $B' \rightarrow [0, 1]$ is a bi-pseudoconvex function of P_s and d, because: (i) $p_{out_{2J}}$ is pseudoconvex in P_s for every fixed d (see Appendix A-B for the proof), (ii) $p_{out_{2J}}$ is a pseudoconvex function of d for every fixed P_s (see Appendix B-B for details), and (iii) feasible region B' defined by $C1$–$C5$ and $C8$ is a convex set (see Section VII-A). ∎

Remark 1: Generalizing the concept of bi-pseudoconvexity, from Lemmas 1, 3, and 4, it may be noted that p_{out_2} is a multi-pseudoconvex (or tri-pseudoconvex) function of P_s, d, and ρ, because it is individually pseudoconvex in each of them (P_s, d, and ρ), with the other two being fixed.

Using Theorem 2 and Lemma 2, the global optimal solution for (J2), (P_s^*, d^*), is obtained using KKT conditions. It may be noted that $C2$ and $C3$ cannot be satisfied at strict equality because they respectively lead to $\rho < 0$ and $p_{out_{2J}} = 1$. Moreover, if $C8$ is satisfied with strict equality, it will lead to $\rho = 0$, which cannot meet $C1$ $\forall$ $\zeta_P > 0$. Thus, only d can be satisfied at its two extremes, i.e., δ and $\frac{D}{\epsilon} - \delta$. So, keeping the boundary constraints $C3$–$C4$ on d implicit, finding the KKT point reduces to finding the critical point of $p_{out_{2J}}(P_s, d)$ if it exists, or finding the minimum $p_{out_{2J}}$ subject to boundary constraints $C2$–$C5$ and $C8$. Minimization of $p_{out_{2J}}$ over both P_s and d simultaneously is nonconvex, however minimization of $p_{out_{2J}}$ with respect to either of them while keeping the other one fixed is pseudoconvex. In this situation, following Theorem 2 and exploiting the merits of bi-pseudoconvexity of $p_{out_{2J}}$, we next propose an alternating optimization algorithm described in Algorithm 1 to find the joint-optimal solution.

Algorithm 1 starts with a feasible starting point given by: $d_0 \triangleq \frac{1}{2}\left(\delta + \max\left\{\delta, \frac{D}{\epsilon} - \left(\frac{\eta a_r P_T}{\zeta_P}\right)^{\frac{1}{l}}\right\}\right)$ and generates an alternating minimization sequence of PA and RP, i.e., $P_{s_1} \rightarrow d_1 \rightarrow P_{s_2} \rightarrow d_2 \rightarrow \cdots$. It returns the joint-optimal PA, RP, and PS (P_s^*, d^*, ρ^*) along with the minimum outage probability $p_{out_{2J}}^*$. It can be observed that the sequence $p_{out}^{(i)}$ is non-increasing and converges to global minimum [40]

TABLE II: Summary of proposed joint cooperative optimization schemes for SWIPT over Rician channels.

Optimization scheme		Features of optimization problem		Remarks on optimal solution(s)
Without direct $\mathcal{S}$-to-$\mathcal{D}$ link	Optimal PA (PA1)	Feasibility condition	$P_s^{th} \geq 0$	$P_s^* = P_{s_1}^0$ implies that higher power is allocated to transmitter of the weaker link, i.e., $P_s^* \geq P_r^*$ if $\frac{a_s}{d^l} \leq \frac{a_r \rho}{(D-d)^l}$ and vice-versa. $P_s^* = P_s^{th}$ implies that sufficient power is allocated to $\mathcal{R}$ to meet ζ_P.
		Objective function	convex	
		Convex constraints	$C1$–$C3$	
	Optimal RP (RP1)	Feasibility condition	$d^{th} \leq D - \delta$	$d^* = d_1^0$ implies that $\mathcal{R}$ is placed closer to $\mathcal{S}$ if $\mathcal{S}$-to-$\mathcal{R}$ link is weaker than the $\mathcal{R}$-to-$\mathcal{D}$ link, $\big(d^* \leq D - d^*$ if $a_s P_s \leq a_r \rho \left(P_T - P_s\right)\big)$. $d^* = d^{th}$ implies that $\mathcal{R}$ is placed sufficiently close to $\mathcal{D}$ to meet ζ_P.
		Objective function	convex	
		Convex constraints	$C1$, $C4$–$C5$	
	Joint optimization of PA, RP, and PS (J1)	Feasibility condition	$\zeta_P \leq \frac{\eta a_r P_T}{\delta^l}$	P_s^* obtained using (40), $d^* = \max\left[\delta, \min\left\{d^J, D - \delta\right\}\right]$, and $\rho^* = 1 - \frac{\zeta_P \left(D - d^*\right)^l}{\eta a_r \left(P_T - P_s^*\right)}$ depend on ζ_P. This leads to a tradeoff between minimized p_{out_1} and underlying ζ_P. Also, if $d^* = d_J$, then $\frac{P_s^*}{P_T} = \frac{d^*}{D}$.
		Objective function	jointly convex	
		Convex constraints	$C2$–$C5$, $C8$	
Optimal PS (PS0) common for without and with direct $\mathcal{S}$-to-$\mathcal{D}$ link		Feasibility condition	$\rho^{th} \geq 0$	$\rho^* = \rho^{th} = 1 - \frac{\zeta_P \left(\frac{D}{\epsilon} - d\right)^l}{\eta a_r \left(P_T - P_s\right)}$ is obtained by solving $C1$ at strict equality. ρ^* and minimized outage probability are respectively decreasing and increasing functions of ζ_P. Also, $\widehat{p_{out_1}}$ is convex in ρ.
		Objective function	pseudoconvex	
		Convex constraints	$C1$, $C6$–$C7$	
With direct $\mathcal{S}$-to-$\mathcal{D}$ link	Optimal PA (PA2)	Feasibility and constraints same as (PA1)		$P_s^* = P_{s_2}^0$ obtained using iterative algorithm provides lower p_{out_2} as compared to $P_s^* = P_s^{th}$ where minimized p_{out_2} increases with ζ_P.
		Objective function	pseudoconvex	
	Optimal RP (RP2)	Feasibility and constraints same as (RP1)		Iterative solution $d^* = d_2^0$ is independent of ζ_P, whereas for $d_2^0 < d^{th}$, both $d^* = d^{th}$ and minimized p_{out_2} increase with increasing ζ_P at $\mathcal{D}$.
		Objective function	pseudoconvex	
	Joint optimization of PA, RP, and PS (J2)	Feasibility and constraints same as (J1)		Optimal solutions (P_s^*, d^*, ρ^*), dependent on ζ_P, are obtained by minimizing $p_{out_{2J}}$ alternatively in P_s and d, with ρ^* in terms of P_s^* and d^*.
		Objective function	multi-pseudoconvex	

because $p_{out_{2J}}$ is individually a pseudoconvex function of P_s and d, and is bounded from below, i.e., $p_{out_{2J}} \geq 0$. Algorithm 1 terminates when $\left(p_{out}^{(i)} - p_{out}^{(i-1)}\right) \leq \xi$, where ξ is an acceptable tolerance. *If $\zeta_P \leq \frac{\eta a_r P_T}{\delta^l}$, then joint-optimal solution returned by Algorithm 1 is a feasible KKT point and, hence, it is the optimal solution. Otherwise, (J2) is infeasible.*

Algorithm 1 Alternating optimization to find joint-optimal PA, RP, and PS to minimize p_{out_2}.

Input: d_0 and ξ
Output: $p_{out_{2J}}^*$, P_s^*, d^*, ρ^*

1: Set $i \leftarrow 0$, $p_{out}^{(0)} \leftarrow p_{out_{2J}}\left(\frac{1}{2}\max\left\{0, P_T - \frac{\zeta_P \left(\frac{D}{\epsilon} - d_0\right)^l}{\eta a_r}\right\}, d_0\right)$
2: **repeat** (Main Loop)
3: Set $i \leftarrow i + 1$
4: Apply CGM with positive PR beta and GS method to find optimal PA satisfying $C2$, $C3$, $C8$, for fixed RP $d = d_{i-1}$ and fixed PS $\rho = 1 - \frac{\zeta_P \left(\frac{D}{\epsilon} - d_{i-1}\right)^l}{\eta a_r \left(P_T - P_s\right)}$:

$$\left\{ P_{s_i} \leftarrow \underset{0 \leq P_s \leq \max\left\{0, P_T - \frac{\zeta_P \left(\frac{D}{\epsilon} - d_{i-1}\right)^l}{\eta a_r}\right\}}{\operatorname{argmin}} p_{out_{2J}}\left(P_s, d_{i-1}\right) \right\}$$

5: Apply CGM with positive PR beta and GS method to find optimal RP satisfying $C4$, $C5$, $C8$, for fixed PA $P_s = P_{s_i}$ and fixed PS $\rho = 1 - \frac{\zeta_P \left(\frac{D}{\epsilon} - d\right)^l}{\eta a_r \left(P_T - P_{s_i}\right)}$:

$$\left\{ d_i \leftarrow \underset{\max\left\{\delta, \frac{D}{\epsilon} - \left(\frac{\eta a_r \left(P_T - P_{s_i}\right)}{\zeta_P}\right)^{\frac{1}{l}}\right\} \leq d \leq \frac{D}{\epsilon} - \delta}{\operatorname{argmin}} p_{out_{2J}}\left(P_{s_i}, d\right) \right\}$$

6: Set $p_{out}^{(i)} \leftarrow p_{out_{2J}}\left(P_{s_i}, d_i\right)$, $p_{out_{2J}}^* \leftarrow p_{out}^{(i)}$,
7: Set $P_s^* \leftarrow P_{s_i}$, $d^* \leftarrow d_i$, $\rho^* \leftarrow 1 - \frac{\zeta_P \left(\frac{D}{\epsilon} - d_i\right)^l}{\eta a_r \left(P_T - P_{s_i}\right)}$
8: **until** $\left(p_{out}^{(i)} - p_{out}^{(i-1)}\right) \leq \xi$

Table II presents a summary of the main analytical results derived in Sections IV-VII. It is worth noting that the unavailability of analytical optimization solutions for direct $\mathcal{S}$-to-$\mathcal{D}$ link case (minimization of p_{out_2}) corroborates the importance of analytical results derived for optimal PA, RP, and PS in no direct link case (minimization of p_{out_1}). These analytical solutions are derived by exploiting the individual and joint convexity of $\widehat{p_{out_1}}$ and $\widehat{p_{out_{1J}}}$ in P_s, d, and ρ.

VIII. Numerical investigation and discussion

Here we analyze the performance of the optimization schemes proposed in Sections IV-VII with the help of numerical examples. We consider $a \triangleq a_s = a_r = a_d = 0.1$, $l = 3$, $\zeta_I = 10$ bits/sec/Hz (outage threshold), $P_T = 40$ dBm, $N_0 = -99.85$ dBm, $K = 6$ dB (Rice factor), $\delta = 1$ m (minimum distance between $\mathcal{S}$–$\mathcal{R}$ or $\mathcal{R}$–$\mathcal{D}$), and $\eta = 0.5$. The $\mathcal{S}$-to-$\mathcal{D}$ distance is: with direct link $D = 20$ m with $\epsilon = 0.8$, and without direct link $D = 100$ m with $\epsilon = 1$. Fixed (non-cooperative) allocations are assumed to be uniform, i.e., $P_s = P_r = 0.5P_T$, $d = 0.5\frac{D}{\epsilon}$, and $\rho = 0.5$ (PS ratio). The tolerance for Algorithm 1 is set as $\xi = 10^{-15}$.

A. Optimal PA for fixed RP and PS [(PA1) and (PA2)]

Figs. 2(a) and 2(b) illustrate the outage performance versus source power, along with optimal PA P_s^* as obtained in (18) and (24), at three different relay positions: $\frac{\epsilon d}{D} \in \{0.25, 0.5, 0.75\}$ with $\rho = 0.5$. In the plots, optimal PA is shown under different harvested power requirements ζ_P. Very low values of $\zeta_P < -30$ dBm, have been considered to observe the performance of the proposed optimization schemes (i) with no energy harvesting requirement (that provides best outage performance) and (ii) for the applications with extremely low energy requirements. However, for most of the practical RFEH applications $\zeta_P \geq -20$ dBm. The minimum p_{out_1} and p_{out_2} (in all 3 cases of RP) is achieved when ζ_P is very low $\big(-32.6$ dBm in Fig. 2(a) and -30 dBm in Fig. 2(b)$\big)$ and, thus, $P_s^* = P_{s_i}^0 < P_s^{th}$ $\forall$ $i = 1, 2$. Also, it is shown that

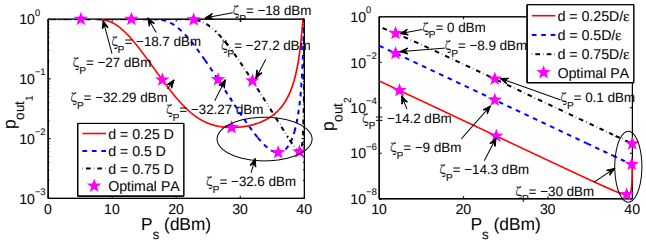

(a) Without direct $\mathcal{S}$-to-$\mathcal{D}$ link (b) With $\mathcal{S}$-to-$\mathcal{D}$ direct link

Fig. 2: Optimal PA with fixed RP and influence of minimum required harvested power ζ_P at $\mathcal{D}$ for $\rho = \frac{1}{2}$.

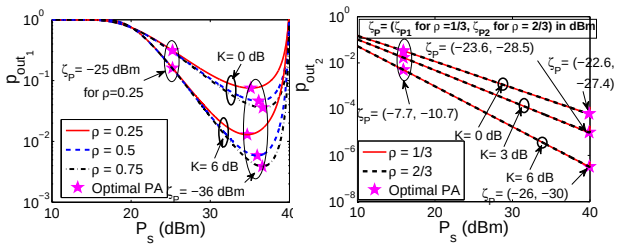

(a) Without direct $\mathcal{S}$-to-$\mathcal{D}$ link (b) With $\mathcal{S}$-to-$\mathcal{D}$ direct link

Fig. 3: Variation of p_{out} with P_s for different ζ_P, ρ, and K values with $\frac{\epsilon d}{D} = 0.5$. Optimal P_s^* is also plotted.

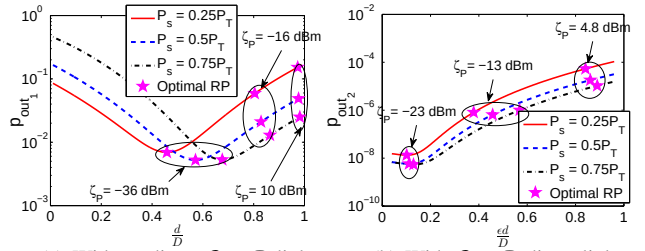

(a) Without direct $\mathcal{S}$-to-$\mathcal{D}$ link (b) With $\mathcal{S}$-to-$\mathcal{D}$ direct link

Fig. 4: Optimal RP with fixed PA and PS, along with the effect of ζ_P on the minimized p_{out_1}, p_{out_2} and optimal RP d^*. Fixed PS considered is: $\rho = 0.5$.

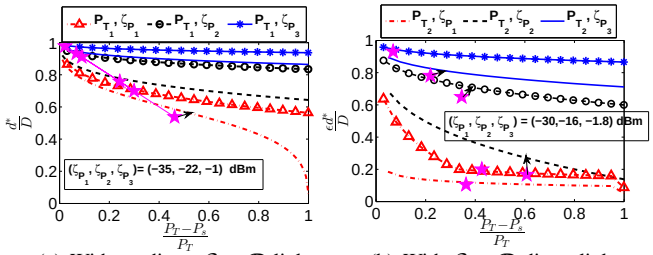

(a) Without direct $\mathcal{S}$-to-$\mathcal{D}$ link (b) With $\mathcal{S}$-to-$\mathcal{D}$ direct link

Fig. 5:Optimal normalized RP versus $\frac{P_T}{P_T}$ with $\left\{P_{T_1}, P_{T_2}\right\}$ $=\{30, 40\}$ dBm and $\zeta_P=\{\zeta_{P_1}, \zeta_{P_2}, \zeta_{P_3}\}$ as mentioned in respective figures. Starred points are joint-optimal solutions.

increasing ζ_P leads to increasing p_{out_i} $\forall$ $i = 1, 2$ resulted by optimal PA as the corresponding P_s^{th} drops below $P_{s_i}^0$.

Remark 2: For no direct $\mathcal{S}$-to-$\mathcal{D}$ link with very low ζ_P, minimum $p_{out_1}^*$ is achieved for $\frac{d}{D} = \frac{1}{2}$. $\frac{d}{D} = \frac{1}{4}$ has the worst outage performance. On the other hand, $p_{out_2}^*$ increases with increased d. However with increasing d, optimal PA to $\mathcal{S}$ increases in both cases to strengthen the weakened $\mathcal{S}$-to-$\mathcal{R}$ link, though this increase in direct $\mathcal{S}$-to-$\mathcal{D}$ link case is relatively lower than without direct link.

Remark 3: For very high P_s, p_{out_1} increases with increased P_s (Figs. 2(a) and 3(a)) due to weakening of $\mathcal{R}$-to-$\mathcal{D}$ link. However, p_{out_2} almost monotonically decreases with increased P_s (Figs. 2(b) and 3(b)) due to the strengthening of both $\mathcal{S}$-to-$\mathcal{D}$ and $\mathcal{S}$-to-$\mathcal{R}$ links.

In Figs. 3(a) and 3(b), the variation of outage versus P_s is plotted for different ρ and K values. For both without and with direct link availability, outage performance improves with increasing ρ and K. However, for high ζ_P, only low ρ provides feasible solution (see Fig. 3(a)) because it allows higher harvested power. Also, as noted in Fig. 3(b), lower ρ helps to meet higher ζ_P.

Remark 4: Impact of ρ on p_{out} is almost negligible when direct link is available (see Fig. 3(b)), though increased K provides significantly improved outage performance in both cases.

Remark 5: The variation of K has negligible impact on P_s^*. However, P_s^* increases with increased ρ, though this increase is negligible for direct link case as compared to no direct link.

B. Optimal RP for fixed PA and PS [(RP1) and (RP2)]

Figs. 4(a) and 4(b) depict p_{out_i} $\forall i = 1, 2$ as a function of relay position for fixed PA and PS ($\rho = 0.5$), along with optimal RP d^*, as given in (29) and (33). Three different fixed PAs have been considered: $P_s \in \{0.25P_T, 0.5P_T, 0.75P_T\}$. Results in Fig. 4(a) show that p_{out_1} achieved by optimal RP decreases with increasing P_s and optimal RP d^* moves closer to $\mathcal{D}$ in no direct link case to strengthen the weaker $\mathcal{R}$-to-$\mathcal{D}$ link. However, this trend is observed more clearly only at high ζ_P for direct link case (see Fig. 4(b)). Moreover, for all values of P_s, p_{out_i} $\forall i = 1, 2$ due to optimal RP increases with increasing ζ_P as in case of optimal PA, because increasing d^{th} goes above d_i^0 $\forall i = 1, 2$. Minimum p_{out_i} is achieved when ζ_P is very low (-36 dBm in Fig. 4(a) and -23 dBm in Fig. 4(b)) and, thus, $d^* = d_i^0 > d^{th}$.

Remark 6: Outage performance of optimal RP for both with and without direct link is better than optimal PA, signifying that optimal RP with fixed PA is a better partially-adaptive scheme.

To get further insights into the performance of optimal RP scheme, we plot the optimal normalized RP $\left(\frac{\epsilon d^*}{D}\right)$ versus relay power ratio $\left(\frac{P_T - P_s}{P_T}\right)$ with $\rho = 0.5, K = 6$ dB, and different P_T and ζ_P in Figs. 5(a) and 5(b) for the two cases of $\mathcal{S}$-to-$\mathcal{D}$ link availability.

Remark 7: With higher P_T and lower ζ_P, optimal RP moves closer to $\mathcal{S}$ with increased PA to $\mathcal{R}$ in order to have lower path loss on $\mathcal{S}$-to-$\mathcal{R}$ link. However, for higher harvested power requirements (increased ζ_P), $\mathcal{R}$ has to be positioned near $\mathcal{D}$, as shown in Figs. 5(a) and 5(b).

Remark 8: With very low ζ_P, optimal RP d^* is close to $\mathcal{S}$ when direct $\mathcal{S}$-to-$\mathcal{D}$ link is available (see Fig. 5(b)) and close to middle position between $\mathcal{S}$ and $\mathcal{D}$ for no direct link case (Fig. 5(a)). A similar trend is observed for optimal RP obtained from the joint optimization scheme. However for high ζ_P, both optimal RP scheme and joint optimization scheme place $\mathcal{R}$ closer to $\mathcal{D}$.

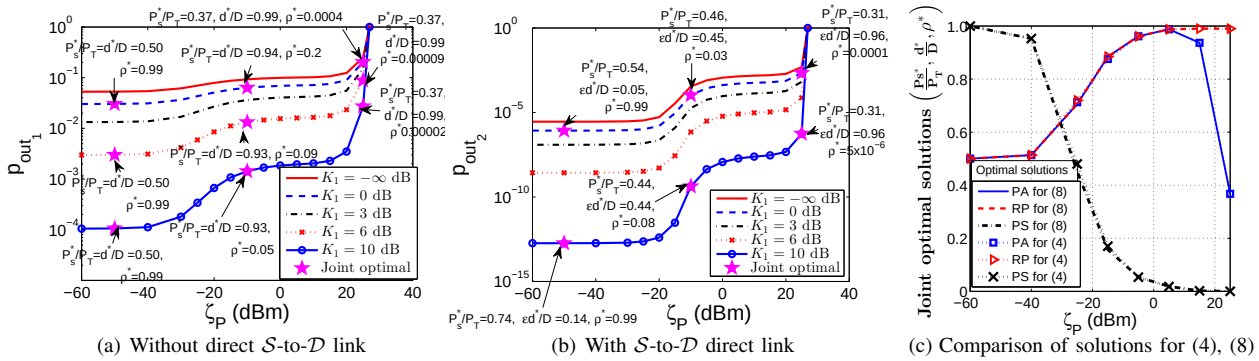

(a) Without direct $\mathcal{S}$-to-$\mathcal{D}$ link (b) With $\mathcal{S}$-to-$\mathcal{D}$ direct link (c) Comparison of solutions for (4), (8)

Fig. 7: (a) and (b) Optimal tradeoff between the minimized outage probability provided by joint optimization scheme and lower bound ζ_P on required harvested power at $\mathcal{D}$. (c) Comparison of jointly-optimized solutions (P_s^*, d^*, ρ^*) that minimize the exact p_{out_1} expression (4) and its tight exponential approximation (8) with varying ζ_P.

C. Optimal PS for fixed PA and RP [(PS0)]

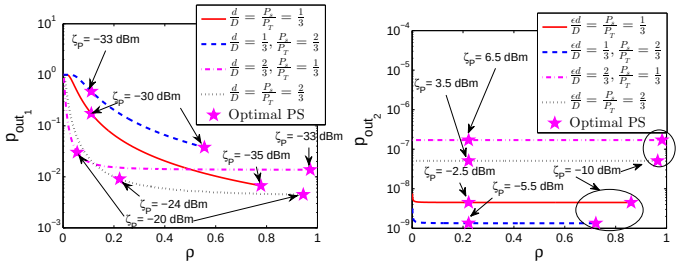

(a) Without direct $\mathcal{S}$-to-$\mathcal{D}$ link (b) With $\mathcal{S}$-to-$\mathcal{D}$ direct link

Fig. 6: Optimal PS with fixed PA and RP, and influence of ζ_P on outage probability and ρ^*.

Figs. 6(a) and 6(b) corroborate the monotonically decreasing behavior of p_{out} with increased ρ for different PA and RP values. Although this decrease in outage probability is significant for no direct link case (Fig. 6(a)), the decrease for direct link case is negligible. The minimized outage probability $p_{out_1}^*$ (and $p_{out_2}^*$) increases and optimal PS ρ^* decreases with increased ζ_P.

Remark 9: For no direct link case (Fig. 6(a)), lower P_s and higher d provide lower p_{out_1}. In contrast, with $\mathcal{S}$-to-$\mathcal{D}$ direct link availability (Fig. 6(b)), higher P_s and lower d provide lower p_{out_2}. However, in both the cases, higher d ($\mathcal{R}$ closer to $\mathcal{D}$) can help to meet higher ζ_P.

Remark 10: The optimal PS for fixed PA and RP scheme plays a more significant role in no direct link case than in the direct $\mathcal{S}$-to-$\mathcal{D}$ link availability case.

D. Joint-optimal PA, RP, and PS [(J1) and (J2)]

The harvested power constraint $C1$ plays a significant role in the outage performance of the joint optimization and other individual optimization schemes. Figs. 7(a) and 7(b) plot the minimized p_{out_i} $\forall i = 1, 2$ obtained by joint optimization scheme for varying ζ_P, under different values of Rice factor $K \in \{-\infty, 0, 3, 6, 10\}$ dB. Total power budget is $P_T = 40$ dBm. The plots are obtained by solving joint optimization problems ((J1) and (J2)) for different ζ_P values, one for each point on the curve. There is no feasible PA, RP, and PS for $\zeta_P > 27$ dBm for both with and without direct link cases for all five considered values of K. As ζ_P is decreased, the minimized p_{out_i} decreases sharply first, then more slowly until $C1$ is no longer active. Finally, a globally Pareto-optimal tradeoff between p_{out_i} and ζ_P is obtained.

The minimum p_{out_i} is achieved when ζ_P is very low (-50 dBm in Fig. 7(a) and -30 dBm in Fig. 7(b)). Results show that increasing ζ_P beyond -40 dBm and -20 dBm for no direct link and with direct link cases, respectively, leads to an increase in minimized outage probability $p_{out_1}^*$ and $p_{out_2}^*$. Also, for the considered numerical examples, Algorithm 1 requires on an average eight iterations for converging to joint-optimal solution within acceptable tolerance.

Remark 11: Without direct $\mathcal{S}$-to-$\mathcal{D}$ link, the normalized optimal PA and RP increase in the same proportion with increased ζ_P for medium and low ζ_P, because as $\mathcal{R}$ is moved closer to $\mathcal{D}$ to meet its ζ_P, P_s is increased to strengthen the weakened $\mathcal{S}$-to-$\mathcal{R}$ link (see Fig. 7(a)).

Remark 12: For very low ζ_P in no direct link case, joint optimization scheme allocates equal power to $\mathcal{S}$ and $\mathcal{R}$ ($\frac{P_s^*}{P_T} \approx 0.5$), and center position ($\frac{\epsilon d^*}{D} \approx 0.5$) is optimal RP. However, $\rho^* \approx 0$ for very high ζ_P, and $\rho^* \approx 1$ for very low ζ_P in both with and without direct link cases.

Remark 13: With direct link availability, optimal PA P_s^* and PS ρ^* provided by joint optimization scheme decreases, whereas optimal RP d^* increases with increased ζ_P. However, there is no trend observed for normalized proportionality of P_s^* and d^*, as in case of no direct link.

Remark 14: Higher K helps to achieve lower p_{out}, signifying that outage performance of joint optimization for SWIPT over Rician channels is better than that over Rayleigh channels. The exact optimization results for Rayleigh fading can be easily generated from our formulation with Rician fading, by substituting $K = 0$ (which implies $\alpha_i = 0.5$ and $\beta_i = 1$ $\forall$ $i = 1, 2, 3$).

Finally, we plot jointly-optimized solutions (obtained numerically using exhaustive three-dimensional search) for minimizing exact p_{out_1} expression (4) in Fig.7(c) and compare them with the analytical solutions derived in Section VII-A to validate the effectiveness of the derived optimal solutions.

Remark 15: Fig. 7(c) shows that the normalized jointly optimal solutions for minimizing (4) *and* (8) *match very tightly with a minor difference of $< 1\%$. This corroborates the consideration of* (5) *as a tight approximation for $Q_1(\cdot, \cdot)$ to obtain analytical and computationally-efficient solutions for*

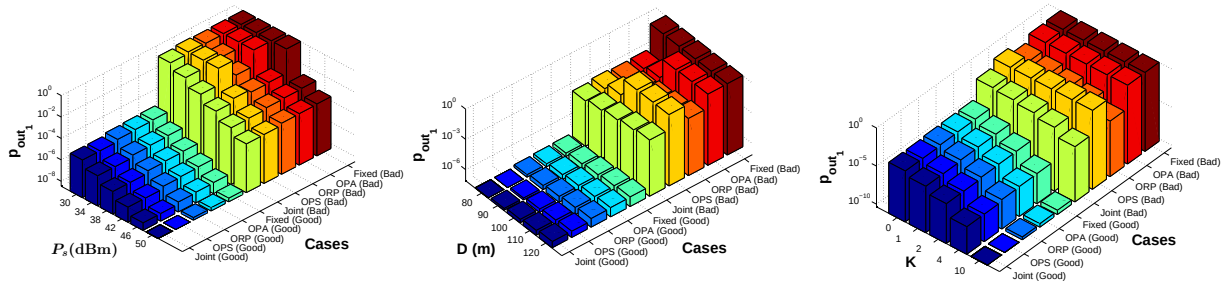

(a) p_{out_1} variation with P_T (b) p_{out_1} variation with D (c) p_{out_1} variation with K

Fig. 8: Outage performance comparison of fixed allocation, optimal PA (OPA), optimal RP (ORP), optimal PS (OPS), and joint optimization schemes under Good and Bad channel conditions for no direct link case.

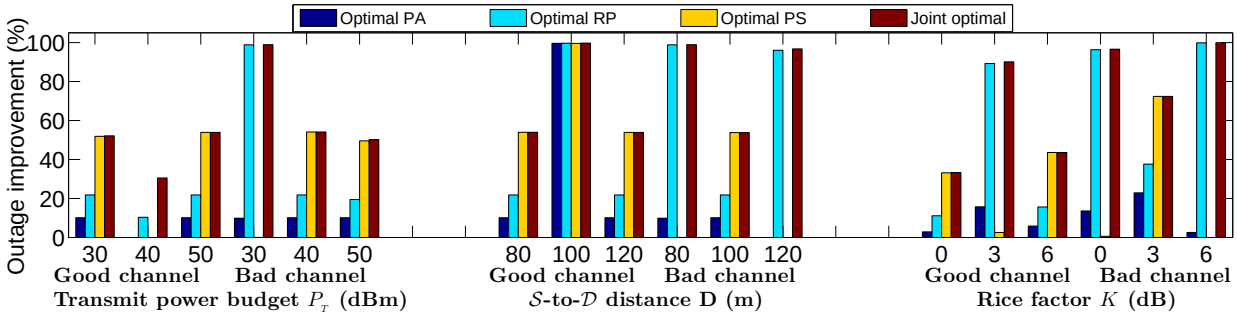

Fig. 9: Performance comparison of the proposed optimization schemes for the no direct link case with fixed allocation scheme for different total power budget P_T, $\mathcal{S}$-to-$\mathcal{D}$ distance D, and Rice factor K.

the proposed optimization schemes in SWIPT.

Remark 16: Due to the log-concavity of $Q_1(a,b)$ in b [41], the obtained results are not much affected by considering other tight approximations and bounds for $Q_1(\cdot,\cdot)$ [26], [33]. However, using (5) *helps in obtaining closed-form optimal solutions for (PA1), (RP1), (PS0), and (J1).*

E. Outage performance comparison

1) No direct $\mathcal{S}$-to-$\mathcal{D}$ link available: Here we present the performance comparison of the proposed optimization schemes against non-cooperative fixed (uniform) allocation scheme. The following cases are considered: (a) varying P_T with D=100 m and $K = 6$ dB; (b) varying D with P_T=40 dBm and $K = 6$ dB; and (c) varying K with P_T=40 dBm and $D = 100$ m, for $\zeta_P = -25$ dBm under two different channel conditions: (i) Good: $a_s = a_r = 0.5, l = 2$ with noise power $= N_0$ and (ii) Bad: $a_s = a_r = 0.1, l = 3$ with noise power $= 2N_0$. Figs. 8(a), 8(b), and 8(c) show that p_{out_1} resulted in each scheme reduces with increased total power P_T budget and Rice factor K values, whereas p_{out_1} increases with increased $\mathcal{S}$-to-$\mathcal{D}$ distance D. The relative performances for different P_T, D, and channel conditions are captured in Fig 9. The average percentage improvement by optimal PA, optimal RP, optimal PS, and joint optimization schemes over the fixed allocation scheme are respectively around 3.86%, 12.61%, 36.18%, and 36.31%, in Good channel conditions, and around 10.15%, 19.45%, 30.68%, and 42.33% in Bad channel conditions (when $p_{out_1} < 1$ for fixed allocation scheme). The imposition of harvested power constraint $C1$ increases the significance of optimal PA, RP, and PS, because fixed allocation sometimes cannot provide a feasible solution as shown in Figs. 8(a) ($P_T \leq 42$ dBm), 8(b), and 8(c) for Bad channel conditions (p_{out_1} for infeasible case is plotted as 1). Even optimal PA and optimal PS schemes are infeasible at lower values of P_T and higher values of D. Due to this, in Bad channel conditions when fixed allocation scheme cannot meet ζ_P and hence $p_{out_1} = 1$ due to its infeasibility, the proposed optimization schemes provide much higher outage improvement. The average percentage improvement by optimal PA, optimal RP, optimal PS, and joint optimization schemes over the fixed allocation scheme with $p_{out_1} = 1$ (infeasibility of fixed allocation scheme) are respectively around 27.25%, 89.42%, 23.55%, and 92.0%.

Remark 17: Impact of the proposed optimization schemes is much more significant when there is no direct link availability because non-cooperative fixed allocation scheme for SWIPT mostly suffers from total outage even for low energy requirements ($\zeta_P \approx -25$ dBm) at $\mathcal{D}$.

Remark 18: Joint optimization scheme always performs the best because it has the highest degree of freedom. The overall order (best to worst) based on the outage performance is: {joint-optimal, optimal PS, optimal RP, optimal PA} for low ζ_P or good channel conditions, and {joint-optimal, optimal RP, optimal PA, optimal PS} for high ζ_P or bad channel conditions.

2) With $\mathcal{S}$-to-$\mathcal{D}$ direct link available: A similar comparison is performed when direct $\mathcal{S}$-to-$\mathcal{D}$ link is available, with $\zeta_P = 0$ dBm. The variations of the following four parameters are studied: (a) transmit power budget P_T; (b) $\mathcal{S}$-to-$\mathcal{D}$ distance D; (c) channel conditions; (d) Rice factor K (see Fig. 10). Under each variation other three parameters are respectively kept fixed as $P_T = 40$ dBm, $D = 20$ m, $K = 6$ dB, and Good channel conditions ($a = 0.5, l = 2, N_0 = -99.85$ dBm). The channel deterioration is implemented by decreasing the channel gains (a_s, a_r, and a_d) and increasing path loss

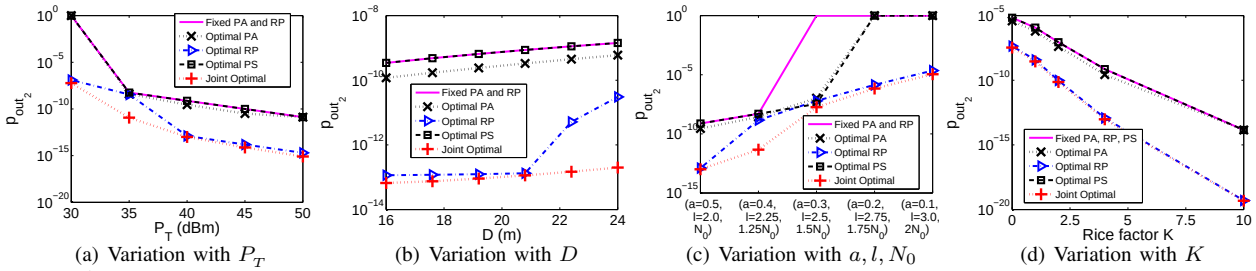

(a) Variation with P_T (b) Variation with D (c) Variation with a, l, N_0 (d) Variation with K

Fig. 10: Outage p_{out_2} performance comparison of the proposed optimization schemes with fixed allocation scheme.

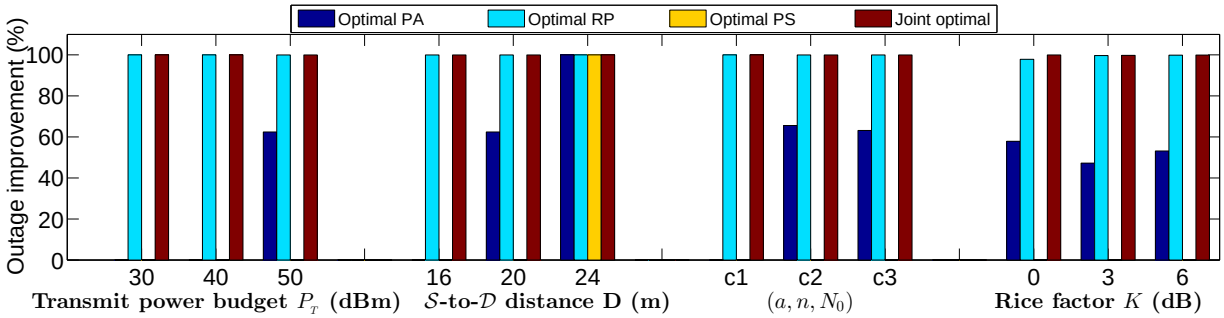

Fig. 11: Performance comparison of the proposed optimization schemes against fixed allocation for direct link case. The percentage improvement results are with respect to p_{out_2} resulted from fixed allocation scheme. Channel condition is varied as: c1$=(0.5, 2, N_0)$ (Good channel), c2$=(0.3, 2.5, 1.5N_0)$, and c3$=(0.1, 3, 2N_0)$ (Bad channel).

exponent l and noise power N_0 with respect to the Good channel conditions (0% deterioration). Figs. 10(a) and 10(d) show that p_{out_2} resulted in each scheme reduces with increased P_T and K, respectively. Instead, Figs. 10(b) and 10(c) show that p_{out_2} increases with increased $\mathcal{S}$-$\mathcal{D}$ distance D and channel deterioration, respectively. In all four variations, joint-optimal PA, RP, and PS has the best outage performance, closely followed by optimal RP with fixed PA and PS. Optimal PA with fixed RP and PS also provides significant outage performance improvement, except being infeasible in certain cases, like very low P_T and very poor channel conditions. However, optimal PS does not provide any practical improvement, except in the case when the fixed allocation scheme results in an infeasible solution (i.e., $p_{out_2} = 1$).

The performance comparison results for direct communication link case are summarized in Fig 11. The average outage performance improvement by optimal PA, optimal RP, optimal PS, and joint optimization schemes over fixed allocation scheme (when it provides a feasible solution, i.e., $p_{out_2} < 1$), are respectively around 43.62%, 99.35%, $7.36 \times 10^{-4}\%$, 99.55%.

Remark 19: The proposed optimization schemes for efficient SWIPT outperform the fixed allocation, which suffers from total outage while meeting energy requirements at $\mathcal{D}$ for low P_T, high D, and poor channel conditions. This efficiency improvement provided by optimal PA, optimal RP, and joint-optimal schemes is much more evident and significant in case of direct $\mathcal{S}$-to-$\mathcal{D}$ link availability (Fig 11) as compared to the no direct link case (Fig 9).

Remark 20: The optimal RP scheme performs much better than optimal PA and optimal PS schemes, and closely follows the best outage performance provided by the jointly optimized scheme for direct link case. However, the scenarios where due to terrain asperities/blockage, $\mathcal{R}$ has to be placed at some specific position, optimal PA is the only efficient optimization scheme possible, because optimal PS does not provide much improvement over fixed allocation scheme.

IX. Concluding Remarks

This paper has investigated the optimization of PA, RP, and PS in two-hop information relaying and energy transfer to minimize the outage probability in SWIPT over Rician channels, subject to total transmit power and harvested power constraints. Two scenarios of source-to-destination ($\mathcal{S}$-to-$\mathcal{D}$) distances, direct $\mathcal{S}$-to-$\mathcal{D}$ link availability and no direct $\mathcal{S}$-to-$\mathcal{D}$ link have been considered. Analytical expressions have been obtained for the four optimization schemes: optimal PA, optimal RP, optimal PS, and joint optimization of PA, RP, and PS for no direct link scenario. In direct link case, joint global optimal PA, RP, and PS has been derived by exploiting multi-pseudoconvexity of outage probability and using an alternating optimization based iterative scheme. Numerical results show that, in general, the joint optimization scheme performs the best, respectively followed by optimal RP and optimal PA. The results also highlight that the direct link case has different outage performance under the four optimization schemes as compared to the case without direct link. For low required harvested power at $\mathcal{D}$ without direct $\mathcal{S}$-to-$\mathcal{D}$ link, optimal RP is close to the center position between $\mathcal{S}$ and $\mathcal{D}$, whereas when direct link is available, optimal RP is closer to $\mathcal{S}$ with higher PA to $\mathcal{S}$. With increasing required harvested power, the normalized optimal PA and RP increase in same proportion in no direct link scenario, whereas no such trend is observed when direct link is available. Also, in general, the optimal PS ratio in no direct link scenario is relatively higher as compared to when direct link is available. The performance of all four

optimization schemes are strongly influenced by the required harvested power due to the tradeoff between the minimized outage probability and the required harvested power at $\mathcal{D}$.

APPENDIX A
INDIVIDUAL PSEUDOCONVEXITY OF OUTAGE PROBABILITY p_{out_2} IN SOURCE POWER P_s

This appendix provides proof of Lemma 1 and the claims made in Theorem 2. In this regard, we first propose Lemma 5 which will be used in proving tri-pseudoconvexity of p_{out_2} in P_s, d, ρ.

Lemma 5: A positive differentiable function f, which is log-concave over a convex set $\mathbb{F}$, is also pseudoconcave over $\mathbb{F}$.

Proof: A function f is concave if and only if $\mathbb{F}$ is convex and it satisfies (A.1) [42].

$$f(y) \leq f(x) + \nabla f(x)^{\intercal}(y-x) \quad \forall x, y \in \mathbb{F}. \tag{A.1}$$

A similar relationship for a positive differentiable log-concave function f is given by (A.2).

$$\log f(y) \leq \log f(x) + \nabla \log f(x)^{\intercal}(y-x) \ \ \forall x, y \in \mathbb{F}. \tag{A.2}$$

A function f is pseudoconcave if $-f$ is pseudoconvex, or $\forall\ x, y \in \mathbb{F}$ (a convex set), $\nabla f(x)^{\intercal}(y-x) \leq 0 \implies f(x) - f(y) \geq 0$. Applying $(\nabla f(x)^{\intercal}(y-x) \leq 0$ in (A.2) and using the positivity of $f(x)$, we obtain: $\log f(y) \leq \log f(x) + \frac{1}{f(x)}\nabla f(x)^{\intercal}(y-x) \leq \log f(x)$, which on using the monotonicity of $\log(\cdot)$ implies $f(y) \leq f(x)$. This proves that log-concavity of a positive differentiable function f implies the pseudoconcavity of f. ∎

A. Proof of Lemma 1: p_{out_2} is pseudoconvex in P_s for fixed RP and PS

First of all we recall a very important property, which states that, for a single variable function the concepts of pseudoconcavity and unimodality are completely equivalent [43]. Using this property, if we show that $\mathcal{G}_1$ is unimodal in the feasible region defined by $C1$–$C3$, it implicitly implies that $\mathcal{G}_1$ is pseudoconcave in P_s. Using $p_{out_2} = 1 - \mathcal{C}_{\gamma_1}(\mathcal{Z})\,\mathcal{C}_{\Upsilon_{02}}(\mathcal{Z})$, we obtain:

$$\begin{aligned} p_{out_2} &= 1 + \mathcal{C}_{\gamma_1}(\mathcal{Z}) \int_{\mathcal{Z}}^{\infty} \left(\frac{\mathrm{d}F_{\gamma_0}(x)}{\mathrm{d}x}\right)\left(\frac{\mathrm{d}F_{\gamma_2}\left(\frac{\mathcal{Z}-x}{\rho}\right)}{\mathrm{d}x}\right)\mathrm{d}x \\ &= 1 - \mathcal{C}_{\gamma_1}(\mathcal{Z}) \int_{\mathcal{Z}}^{\infty} \mathcal{G}_1(P_s, d, \rho, x)\,\mathrm{d}x. \end{aligned} \tag{A.3}$$

Here $\mathcal{G}_1(P_s, d, \rho, x) \triangleq \left[\frac{\alpha_0'\beta_0\alpha_2''\beta_2}{x(\mathcal{Z}-x)}\left(\frac{D^l}{a_d P_s}\right)^{\beta_0}\left(\frac{\left(\frac{D}{\epsilon}-d\right)^l}{\rho a_r\left(P_T-P_s\right)}\right)^{\beta_2} \times e^{-\alpha_0'\left(\frac{D^l}{a_d P_s}\right)^{\beta_0} - \alpha_2''\left(\frac{\left(\frac{D}{\epsilon}-d\right)^l}{\rho a_r\left(P_T-P_s\right)}\right)^{\beta_2}}\right]$, $\alpha_0' = e^{\phi\left(\sqrt{2K_0}\right)}\left(2(K_0+1)N_0 x\right)^{\beta_0}$ and $\alpha_2'' = e^{\phi\left(\sqrt{2K_2}\right)}\left(2(K_2+1)N_0(\mathcal{Z}-x)\right)^{\beta_2}$.

Next we find the critical point of $\mathcal{G}_1$ in P_s by solving $\frac{\partial \mathcal{G}_1}{\partial P_s} = 0$. Except the trivial case with $\alpha_0'\left(\frac{D^l}{a_d P_s}\right)^{\beta_0} = 1$ and $\alpha_2''\left(\frac{\left(\frac{D}{\epsilon}-d\right)^l}{\rho a_r\left(P_T-P_s\right)}\right)^{\beta_2} = 1$, critical point of $\mathcal{G}_1$ is obtained by numerically solving (A.4). Let the solution of (A.4) be $\overline{P_s}$. Now if $\alpha_0'\left(\frac{D^l}{a_d P_s}\right)^{\beta_0} > 1$ and $\alpha_2''\left(\frac{\left(\frac{D}{\epsilon}-d\right)^l}{\rho a_r\left(P_T-P_s\right)}\right)^{\beta_2} > 1$, $\mathcal{G}_1$ is respectively an increasing and a decreasing function of P_s for $P_s < \overline{P_s}$ and $P_s > \overline{P_s}$. This behavior gets reversed if $\alpha_0'\left(\frac{D^l}{a_d P_s}\right)^{\beta_0} < 1$ and $\alpha_2''\left(\frac{\left(\frac{D}{\epsilon}-d\right)^l}{\rho a_r\left(P_T-P_s\right)}\right)^{\beta_2} < 1$. This proves that $\mathcal{G}_1$ is a pseudoconcave function [43] of P_s. As integration preserves the pseudoconcavity of positive pseudoconcave function [44], pseudoconcavity of $\mathcal{G}_1$ in P_s also implies pseudoconcavity of $\mathcal{C}_{\Upsilon_{02}}(\mathcal{Z}) = \int_{\mathcal{Z}}^{\infty}\mathcal{G}_1\mathrm{d}x$. Apart from this, since $\frac{\partial^2 \log\left[\mathcal{C}_{\gamma_1}(\mathcal{Z})\right]}{\partial P_s^2} = -\frac{\alpha_1\beta_1(\beta_1+1)d^{\beta_1 l}}{a_s^{\beta_1}P_s^{\beta_1+2}} < 0\ \forall\ P_s > 0$, it implies log-concavity, and hence pseudoconcavity of $\mathcal{C}_{\gamma_1}$ in P_s on applying Lemma 5. Also, it may be noted that the product of two positive pseudoconcave functions is also pseudoconcave [43]. Hence, $\mathcal{C}_{\gamma_1}(\mathcal{Z})\,\mathcal{C}_{\Upsilon_{02}}(\mathcal{Z})$ is pseudoconcave in P_s, which implies pseudoconvexity of p_{out_2} in P_s.

B. $p_{out_{2J}}$ is pseudoconvex in P_s for fixed RP

As $p_{out_{2J}}$ can be obtained from p_{out_2} by substituting $\rho = 1 - \frac{\zeta_P\left(\frac{D}{\epsilon}-d\right)^l}{\eta a_r\left(P_T-P_s\right)}$, the proof of pseudoconvexity of $p_{out_{2J}}$ in P_s is similar as the proof of pseudoconvexity of p_{out_2}.

$$\begin{aligned} p_{out_{2J}} &= 1 - \mathcal{C}_{\gamma_1}(\mathcal{Z})\left[1 - \int_0^{\mathcal{Z}} \frac{\mathrm{d}F_{\gamma_0}(x)}{\mathrm{d}x} F_{\gamma_2}\left(\frac{\eta a_r\left(P_T-P_s\right)(\mathcal{Z}-x)}{\eta a_r\left(P_T-P_s\right) - \zeta_P\left(\frac{D}{\epsilon}-d\right)^l}\right)\mathrm{d}x\right] \\ &= 1 - \mathcal{C}_{\gamma_1}(\mathcal{Z}) \int_{\mathcal{Z}}^{\infty} \widehat{\mathcal{G}_1}(P_s, d, x)\,\mathrm{d}x \end{aligned} \tag{A.5}$$

where $\widehat{\mathcal{G}_1}(P_s, d, x) \triangleq \frac{\alpha_0'\beta_0\alpha_2''\beta_2}{x(\mathcal{Z}-x)}\left(\frac{D^l}{a_d P_s}\right)^{\beta_0}\left(\frac{\eta\left(\frac{D}{\epsilon}-d\right)^l}{\eta a_r\left(P_T-P_s\right)-\zeta_P\left(\frac{D}{\epsilon}-d\right)^l}\right)^{\beta_2} \times e^{-\alpha_0'\left(\frac{D^l}{a_d P_s}\right)^{\beta_0} - \alpha_2''\left(\frac{\eta\left(\frac{D}{\epsilon}-d\right)^l}{\eta a_r\left(P_T-P_s\right)-\zeta_P\left(\frac{D}{\epsilon}-d\right)^l}\right)^{\beta_2}}$. The critical point of $\widehat{\mathcal{G}_1}$ in P_s (i.e., $\frac{\partial \widehat{\mathcal{G}_1}}{\partial P_s} = 0$) is obtained by numerically solving (A.6). Let the solution of (A.6) be $\widehat{P_s}$. Now, similar to the observation in Appendix A-A, if $\alpha_0'\left(\frac{D^l}{a_d P_s}\right)^{\beta_0} > 1$ and $\alpha_2''\left(\frac{\eta\left(\frac{D}{\epsilon}-d\right)^l}{\eta a_r\left(P_T-P_s\right)-\zeta_P\left(\frac{D}{\epsilon}-d\right)^l}\right)^{\beta_2} > 1$, $\widehat{\mathcal{G}_1}$ is respectively an increasing and a decreasing function of P_s for $P_s < \widehat{P_s}$ and $P_s > \widehat{P_s}$. The function behavior gets reversed for $\alpha_0'\left(\frac{D^l}{a_d P_s}\right)^{\beta_0} < 1$ and $\alpha_2''\left(\frac{\eta\left(\frac{D}{\epsilon}-d\right)^l}{\eta a_r\left(P_T-P_s\right)-\zeta_P\left(\frac{D}{\epsilon}-d\right)^l}\right)^{\beta_2} < 1$. This proves that $\widehat{\mathcal{G}_1}$ is a pseudoconcave function of P_s. This along with the discussions related to the integration and product of positive pseudoconcave functions, as mentioned in Appendix A-A, proves pseudoconvexity of $p_{out_{2J}}$ in P_s.

APPENDIX B
INDIVIDUAL PSEUDOCONVEXITY OF OUTAGE PROBABILITY p_{out_2} IN $\mathcal{S}$-TO-$\mathcal{R}$ DISTANCE d

This appendix provides proofs for Lemma 3 and the claims made in Theorem 2 regarding pseudoconvexity of $p_{out_{2J}}$ in d for fixed PA. We note that, p_{out_2} in (A.3) can be rewritten as:

$$\begin{aligned} p_{out_2} &= 1 - \mathcal{C}_{\gamma_1}(\mathcal{Z})\,\mathcal{C}_{\Upsilon_{02}}(\mathcal{Z}) = 1 - \mathcal{C}_{\gamma_1}(\mathcal{Z})\left[\mathcal{C}_{\gamma_0}(\mathcal{Z}) \right. \\ &\quad \left. + \int_0^{\mathcal{Z}} \frac{\mathrm{d}F_{\gamma_0}(x)}{\mathrm{d}x}\mathcal{C}_{\gamma_2}\left(\frac{\mathcal{Z}-x}{\rho}\right)\mathrm{d}x\right]. \end{aligned} \tag{B.1}$$

$$P_T\left[-1+\alpha_0'\left(\frac{D^l}{a_dP_s}\right)^{\beta_0}\right]=P_s\left[-2+\alpha_0'\left(\frac{D^l}{a_dP_s}\right)^{\beta_0}+\alpha_2''\left(\frac{\left(\frac{D}{\epsilon}-d\right)^l}{\rho a_r\left(P_T-P_s\right)}\right)^{\beta_2}\right]. \tag{A.4}$$

$$\left(\alpha_0'\left(\frac{D^l}{a_dP_s}\right)^{\beta_0}-1\right)\left(\eta a_r\left(P_T-P_s\right)-\zeta_P\left(\frac{D}{\epsilon}-d\right)^l\right)=\frac{\beta_2}{\beta_0}\eta a_rP_s\left(\alpha_2''\left(\frac{\eta\left(\frac{D}{\epsilon}-d\right)^l}{\eta a_r\left(P_T-P_s\right)-\zeta_P\left(\frac{D}{\epsilon}-d\right)^l}\right)^{\beta_2}-1\right) \tag{A.6}$$

$\frac{\partial^2\log\left[\mathcal{C}_{\gamma_1}(\mathcal{Z})\right]}{\partial d^2}=-\frac{\alpha_1\beta_1l(\beta_1l-1)d^{\beta_1l-2}}{(a_sP_s)^{\beta_1}}<0\ \forall\ (d>0)\wedge(l>1)$ implies log-concavity of d in $\mathcal{C}_{\gamma_1}(\mathcal{Z})$.

A. Proof of Lemma 3: p_{out_2} is pseudoconvex in d for fixed PA and PS

Let $\mathcal{G}_2\left(P_s,d,\rho,x\right)\triangleq\frac{\mathrm{d}F_{\gamma_0}(x)}{\mathrm{d}x}\mathcal{C}_{\gamma_2}\left(\frac{\mathcal{Z}-x}{\rho}\right)=\frac{\alpha_0'\beta_0}{x}\left(\frac{D^l}{a_dP_s}\right)^{\beta_0}e^{-\alpha_0'\left(\frac{D^l}{a_dP_s}\right)^{\beta_0}-\alpha_2''\left(\frac{\left(\frac{D}{\epsilon}-d\right)^l}{\rho a_r\left(P_T-P_s\right)}\right)^{\beta_2}}$. So using $\mathcal{G}_2$ definition in (B.1),

$$\mathcal{C}_{\Upsilon_{02}}\left(\mathcal{Z}\right)=\mathcal{C}_{\gamma_0}\left(\mathcal{Z}\right)+\int_0^{\mathcal{Z}}\mathcal{G}_2\left(P_s,d,\rho,x\right)\mathrm{d}x. \tag{B.2}$$

$\frac{\partial^2\log\mathcal{G}_2}{\partial d^2}=-\frac{\alpha_2''\beta_2l(\beta_2l-1)\left(\frac{D}{\epsilon}-d\right)^{\beta_2l-2}}{\left(\rho a_r\left(P_T-P_s\right)\right)^{\beta_2}}<0$ implies that $\mathcal{G}_2$ is a log-concave function of d. Since the log-concavity of a positive function is preserved under integration [42], [45], we note that $\int_0^{\mathcal{Z}}\mathcal{G}_2\left(P_s,d,\rho,x\right)\mathrm{d}x$ is also log-concave in d. Since $\mathcal{C}_{\gamma_0}\left(\mathcal{Z}\right)=e^{-\alpha_0\left(\frac{D^l}{a_dP_s}\right)^{\beta_0}}$ is independent of d and log-concavity is preserved under affine transformation, $\mathcal{C}_{\Upsilon_{02}}\left(\mathcal{Z}\right)$ is log-concave in d. As the product of two log-concave functions is also log-concave [42], it results in log-concavity of $\mathcal{C}_{\gamma_1}\left(\mathcal{Z}\right)\mathcal{C}_{\Upsilon_{02}}\left(\mathcal{Z}\right)$, which by using Lemma 5 implies pseudoconvexity of p_{out_2} in d.

B. $p_{out_{2J}}$ is pseudoconvex in d for fixed PA

The expression of $p_{out_{2J}}$ in terms of F_{γ_0}, $\mathcal{C}_{\gamma_0}$, $\mathcal{C}_{\gamma_1}$, and $\mathcal{C}_{\gamma_2}$ is given as:

$$p_{out_{2J}}=1-\mathcal{C}_{\gamma_1}\left(\mathcal{Z}\right)\left[\mathcal{C}_{\gamma_0}\left(\mathcal{Z}\right)+\int_0^{\mathcal{Z}}\frac{\mathrm{d}F_{\gamma_0}\left(x\right)}{\mathrm{d}x}\mathcal{C}_{\gamma_2}\left(\frac{\eta a_r\left(P_T-P_s\right)\left(\mathcal{Z}-x\right)}{\eta a_r\left(P_T-P_s\right)-\zeta_P\left(\frac{D}{\epsilon}-d\right)^l}\right)\mathrm{d}x\right]. \tag{B.3}$$

Let $\widehat{\mathcal{G}_2}\left(P_s,d,\rho,x\right)\triangleq\frac{\mathrm{d}F_{\gamma_0}(x)}{\mathrm{d}x}\mathcal{C}_{\gamma_2}\left(\frac{\mathcal{Z}-x}{\rho}\right)=\frac{\alpha_0'\beta_0}{x}\left(\frac{D^l}{a_dP_s}\right)^{\beta_0}e^{-\alpha_0'\left(\frac{D^l}{a_dP_s}\right)^{\beta_0}-\alpha_2''\left(\frac{\eta\left(\frac{D}{\epsilon}-d\right)^l}{\eta a_r\left(P_T-P_s\right)-\zeta_P\left(\frac{D}{\epsilon}-d\right)^l}\right)^{\beta_2}}$.

Hence, $\frac{\partial^2\log\widehat{\mathcal{G}_2}}{\partial d^2}=-\left[\frac{\eta^{\beta_2+1}(\beta_2l-1)a_r\left(P_T-P_s\right)-\zeta_P(l+1)\left(\frac{D}{\epsilon}-d\right)^l}{\left[\eta a_r\left(P_T-P_s\right)-\zeta_P\left(\frac{D}{\epsilon}-d\right)^l\right]^{\beta_2+2}}\times\alpha_2''\beta_2\eta la_r\left(P_T-P_s\right)\left(\frac{D}{\epsilon}-d\right)^{\beta_2l-2}\right]<0\ \forall\left\{d\ \middle|\ \left(d\le\frac{D}{\epsilon}\right)\wedge\left(P_s\le P_T\right)\wedge\left(l\ge1\right)\wedge\left(\frac{\zeta_P\left(\frac{D}{\epsilon}-d\right)^l}{\eta a_r\left(P_T-P_s\right)}\le1\right)\right\}$. Similar to Appendix B-A, using Lemma 5, independence of $\mathcal{C}_{\gamma_0}$ in d, log-concavity preservation properties of affine transformation, integration, and product of log-concave functions, it is inferred that $p_{out_{2J}}$ is pseudoconvex in d.

Appendix C
Proof of Lemma 4: Outage Probability p_{out_2} is Pseudoconvex in PS Ratio ρ

To show pseudoconvexity of $p_{out_2}=1-\mathcal{C}_{\gamma_1}\left(\mathcal{Z}\right)\mathcal{C}_{\Upsilon_{02}}\left(\mathcal{Z}\right)$ where $\mathcal{C}_{\Upsilon_{02}}\left(\mathcal{Z}\right)$ defined in (B.2), we first prove log-concavity of $\mathcal{G}_2$ in ρ, followed by the pseudoconcavity of $\mathcal{C}_{\gamma_1}\left(\mathcal{Z}\right)\mathcal{C}_{\Upsilon_{02}}\left(\mathcal{Z}\right)$ in ρ.

$\frac{\partial^2\log\mathcal{G}_2}{\partial\rho^2}=-\frac{\alpha_2''\beta_2(\beta_2+1)}{\rho^2}\left[\frac{\left(\frac{D}{\epsilon}-d\right)^l}{\rho a_r\left(P_T-P_s\right)}\right]^{\beta_2}<0\ \forall\left\{\rho\ \middle|\ (\rho>0)\wedge\left(d\le\frac{D}{\epsilon}\right)\wedge\left(P_s\le P_T\right)\right\}$ implies that $\mathcal{G}_2$ is a log-concave function of ρ. Since $\mathcal{C}_{\gamma_0}\left(\mathcal{Z}\right)$ and $\mathcal{C}_{\gamma_1}\left(\mathcal{Z}\right)$ are independent of ρ, and log-concavity is preserved under affine transformation [42], integration [45], and positive scalar multiplication, it can be inferred from (B.1) and (B.2) that $\mathcal{C}_{\gamma_1}(\mathcal{Z})\,\mathcal{C}_{\Upsilon_{02}}(\mathcal{Z})$ is log-concave in ρ. This, by using Lemma 5, also implies that $\mathcal{C}_{\gamma_1}(\mathcal{Z})\,\mathcal{C}_{\Upsilon_{02}}(\mathcal{Z})$ is pseudoconcave in ρ. Hence, p_{out_2} is pseudoconvex in ρ.

Appendix D
Proof of Joint Convexity of Approximated Outage Probability $\widehat{p_{out_{1J}}}$ with $\rho=\rho^{th}$

$\widehat{p_{out_{1J}}}$ can be represented as a sum of two functions $g_1\left(P_s,d\right)=\alpha_1\left(\frac{d^l}{a_sP_s}\right)^{\beta_1}$ and $g_2\left(P_s,d\right)=\alpha_2\left(\frac{\eta\left(\frac{D}{\epsilon}-d\right)^l}{\eta a_r\left(P_T-P_s\right)-\zeta_P\left(\frac{D}{\epsilon}-d\right)^l}\right)^{\beta_2}$. Joint convexity of $\widehat{p_{out_{1J}}}$ in P_s and d can be proved by showing the convexity of g_1 and g_2. The Hessian matrix of g_1 is given as: $H\left(g_1\right)=\begin{bmatrix}\frac{\partial^2g_1}{\partial P_s^2}&\frac{\partial^2g_1}{\partial P_s\partial d}\\\frac{\partial^2g_1}{\partial d\partial P_s}&\frac{\partial^2g_1}{\partial d^2}\end{bmatrix}=\begin{bmatrix}\frac{\alpha_1\beta_1(\beta_1+1)d^{\beta_1l}}{a_s^{\beta_1}P_s^{\beta_1+2}}&-\frac{\alpha_1\beta_1^2ld^{\beta_1l-1}}{a_s^{\beta_1}P_s^{\beta_1+1}}\\-\frac{\alpha_1\beta_1^2ld^{\beta_1l-1}}{a_s^{\beta_1}P_s^{\beta_1+1}}&\frac{\alpha_1\beta_1l(\beta_1l-1)d^{\beta_1l-2}}{(a_sP_s)^{\beta_1}}\end{bmatrix}$. The determinant $\det\left[H\left(g_1\right)\right]=\frac{\alpha_1^2\beta_1^2l(\beta_1(l-1)-1)d^{2(\beta_1l-1)}}{a_s^{2\beta_1}P_s^{2(\beta_1+1)}}\ge0$, and $\frac{\partial^2g_1}{\partial P_s^2},\frac{\partial^2g_1}{\partial d^2}\ge0\ \forall\left\{(P_s,d)\mid(d\ge0)\wedge(P_s\ge0)\wedge(l>1)\right\}$. This proves joint-convexity of g_1 in P_s and d. Similarly, on computing Hessian of g_2, we observe that $\frac{\partial^2g_2}{\partial P_s^2}=\frac{\alpha_2\beta_2(\beta_2+1)(a_r\eta)^2\left[\eta\left(\frac{D}{\epsilon}-d\right)^l\right]^{\beta_2}}{\left[a_r\eta\left(P_T-P_s\right)-\zeta_P\left(\frac{D}{\epsilon}-d\right)^l\right]^{2\beta_2}}$, $\frac{\partial^2g_2}{\partial d^2}=\frac{\alpha_2\beta_2\eta^{\beta_2+1}la_r\left(P_T-P_s\right)\left(\frac{D}{\epsilon}-d\right)^{\beta_2l-2}\left(a_r\eta(\beta_2l-1)\left(P_T-P_s\right)+\zeta_P(l+1)(\frac{D}{\epsilon}-d)^l\right)}{\left[a_r\eta\left(P_T-P_s\right)-\zeta_P(\frac{D}{\epsilon}-d)^l\right]^{\beta_2+2}}$, and $\det\left[H\left(g_2\right)\right]=\left[\frac{a_r\eta(\beta_2(l-1)-1)\left(P_T-P_s\right)+\zeta_Pl\left(\frac{D}{\epsilon}-d\right)^l}{\left(a_r\eta\left(P_T-P_s\right)-\zeta_P(\frac{D}{\epsilon}-d)^l\right)^3}\times(\alpha_2\beta_2a_r)^2\,\eta^{2(\beta_2+1)}l\left(\frac{D}{\epsilon}-d\right)^{2(\beta_2-1)}\right]\ge0\ \forall\left\{(P_s,d)\ \middle|\ \left(d\le\frac{D}{\epsilon}\right)\wedge(P_s\le P_T)\wedge(l\ge2)\right\}$. This implies convexity of $\widehat{p_{out_{1J}}}$ in P_s and d.

APPENDIX E
PROOF OF JOINT CONVEXITY OF CONSTRAINT $C8$ IN (J1) AND (J2)

In this appendix, we prove the joint convexity of $g_{C8} = \frac{\zeta_P\left(\frac{D}{\epsilon}-d\right)^l}{\eta a_r\left(P_T-P_s\right)} - 1$ in P_s and d. The determinant of the Hessian matrix of g_{C8} is $\det\left[H\left(g_{C8}\right)\right] = \frac{\zeta_P^2(l-2)l\left(\frac{D}{\epsilon}-d\right)^{2(l-1)}}{\eta^2 a_r^2\left(P_T-P_s\right)^4} \geq 0 \; \forall \left\{(P_s,d) \;\middle|\; (d \leq \frac{D}{\epsilon}) \wedge \;\; (P_s \leq P_T) \wedge (l \geq 2)\right\}$. This along with non-negativity of $\frac{\partial^2 g_{C8}}{\partial P_s^2} = \frac{2\zeta_P\left(\frac{D}{\epsilon}-d\right)^l}{\eta a_r\left(P_T-P_s\right)^3}$ and $\frac{\partial^2 g_{C8}}{\partial d^2} = \frac{\zeta_P(l-1)l\left(\frac{D}{\epsilon}-d\right)^{l-2}}{\eta a_r\left(P_T-P_s\right)}$ for $P_s \leq P_T$, $d \leq \frac{D}{\epsilon}$, and $l \geq 1$ implies joint-convexity of g_{C8} in P_s and d.

REFERENCES

[1] M. Hasna and M.-S. Alouini, "Optimal power allocation for relayed transmissions over rayleigh-fading channels," *IEEE Trans. Wireless Commun.*, vol. 3, no. 6, pp. 1999–2004, Nov. 2004.

[2] S. Ikki, M. Uysal, and M. Ahmed, "Joint optimization of power allocation and relay location for decode-and-forward dual-hop systems over Nakagami-m fading channels," in *Proc. IEEE GLOBECOM*, Honolulu, HI, USA, Nov. 2009.

[3] S. Ikki and S. Aissa, "A study of optimization problem for amplify-and-forward relaying over weibull fading channels with multiple antennas," *IEEE Commun. Lett.*, vol. 15, no. 11, pp. 1148–1151, Nov. 2011.

[4] M. Wang and Z. Zhong, "Optimal power allocation and relay location for decode-and-forward dual-hop systems over weibull fading channels," in *Proc. IWCMC*, Limassol, Cyprus, Aug. 2012, pp. 240–244.

[5] C. Kundu and R. Bose, "Joint optimal power allocation and relay location for amplify-and-forward multihop relaying over lognormal channel," in *Proc. IEEE VTC Spring*, Dresden, Germany, June 2013.

[6] R. Cao and L. Yang, "The affecting factors in resource optimization for cooperative communications: A case study," *IEEE Trans. Wireless Commun.*, vol. 11, no. 12, pp. 4351–4361, Dec. 2012.

[7] I. Kim and D. Kim, "Outage-constrained source-sum-power minimization in multiple-sensor single-DF-relay networks with direct links," in *Proc. IEEE Int. Conf. on Ubiquitous and Future Netw. (ICUFN)*, Shanghai, 2014, pp. 113–114.

[8] I. Kim and D. Kim, "Outage-constrained source-sum-power minimization in multiple-sensor single-DF-relay networks," *IEEE Commun. Lett.*, vol. 17, no. 7, pp. 1388–1391, July 2013.

[9] L. Varshney, "Transporting information and energy simultaneously," in *Proc. IEEE Int. Symp. Inf. Theory (ISIT)*, Toronto, Canada, July 2008, pp. 1612–1616.

[10] P. Grover and A. Sahai, "Shannon meets Tesla: Wireless information and power transfer," in *Proc. IEEE Int. Symp. Inf. Theory (ISIT)*, Austin, TX, Jun. 2010, pp. 2363–2367.

[11] R. Zhang and C. K. Ho, "MIMO broadcasting for simultaneous wireless information and power transfer," *IEEE Trans. Wireless Commun.*, vol. 12, no. 5, pp. 1989–2001, May 2013.

[12] A. Nasir, X. Zhou, S. Durrani, and R. Kennedy, "Relaying protocols for wireless energy harvesting and information processing," *IEEE Trans. Wireless Commun.*, vol. 12, no. 7, pp. 3622–3636, July 2013.

[13] C. Zhong, H. Suraweera, G. Zheng, I. Krikidis, and Z. Zhang, "Wireless information and power transfer with full duplex relaying," *IEEE Trans. Commun.*, vol. 62, no. 10, pp. 3447–3461, Oct. 2014.

[14] Z. Ding, S. Perlaza, I. Esnaola, and H. Poor, "Power allocation strategies in energy harvesting wireless cooperative networks," *IEEE Trans. Wireless Commun.*, vol. 13, no. 2, pp. 846–860, Feb. 2014.

[15] G. Zhu, C. Zhong, H. Suraweera, G. Karagiannidis, Z. Zhang, and T. Tsiftsis, "Wireless information and power transfer in relay systems with multiple antennas and interference," *IEEE Trans. Commun.*, vol. 63, no. 4, pp. 1400–1418, Apr. 2015.

[16] I. Krikidis, "Simultaneous information and energy transfer in large-scale networks with/without relaying," *IEEE Trans. Commun.*, vol. 62, no. 3, pp. 900–912, Mar. 2014.

[17] Z. Ding, I. Krikidis, B. Sharif, and H. Poor, "Wireless information and power transfer in cooperative networks with spatially random relays," *IEEE Trans. Wireless Commun.*, vol. 13, no. 8, pp. 4440–4453, Aug. 2014.

[18] D. Michalopoulos, H. Suraweera, and R. Schober, "Relay selection for simultaneous information transmission and wireless energy transfer: A tradeoff perspective," *IEEE J. Sel. Areas Commun.*, vol. 33, no. 8, pp. 1578–1594, Aug 2015.

[19] Z. Ding, C. Zhong, D. Ng, M. Peng, H. Suraweera, R. Schober, and H. Poor, "Application of smart antenna technologies in simultaneous wireless information and power transfer," *IEEE Commun. Mag.*, vol. 53, no. 4, pp. 86–93, Apr. 2015.

[20] L. Liu, R. Zhang, and K.-C. Chua, "Wireless information and power transfer: A dynamic power splitting approach," *IEEE Trans. Commun.*, vol. 61, no. 9, pp. 3990–4001, September 2013.

[21] H. Suraweera, G. Karagiannidis, and P. Smith, "Performance analysis of the dual-hop asymmetric fading channel," *IEEE Trans. Wireless Commun.*, vol. 8, no. 6, pp. 2783–2788, June 2009.

[22] S. De and R. Singhal, "Toward uninterrupted operation of wireless sensor networks," *IEEE Computer Mag.*, vol. 45, no. 9, pp. 24–30, Sep. 2012.

[23] D. Mishra, K. Kaushik, S. De, S. Basagni, K. Chowdhury, S. Jana, and W. Heinzelman, "Implementation of multi-path energy routing," in *Proc. IEEE PIMRC*, Washington D.C., USA, Sep. 2014.

[24] K. Kaushik, D. Mishra, S. De, S. Basagni, W. Heinzelman, K. Chowdhury, and S. Jana, "Experimental demonstration of multi-hop RF energy transfer," in *Proc. IEEE PIMRC*, London, UK, Sep. 2013, pp. 538–542.

[25] M. Yu, J. Li, and H. Sadjadpour, "Amplify-forward and decode-forward: The impact of location and capacity contour," in *Proc. IEEE Military Commun. Conf. (MILCOM)*, Atlantic City, NJ, Oct. 2005, pp. 1609–1615 Vol. 3.

[26] M. K. Simon and M.-S. Alouini, *Digital communication over fading channels*, 2nd ed. New York, USA: Wiley, 2005.

[27] C. A. Balanis, *Antenna theory: analysis and design*. John Wiley & Sons, 2012.

[28] D. Mishra, S. De, S. Jana, S. Basagni, K. Chowdhury, and W. Heinzelman, "Smart RF energy harvesting communications: Challenges and opportunities," *IEEE Commun. Mag.*, vol. 53, no. 4, pp. 70–78, Apr. 2015.

[29] Powercast. [Online]. Available: http://www.powercastco.com

[30] FCC codes of regulation, part 15. [Online]. Available: http://www.access.gpo.gov/nara/cfr/waisidx03/

[31] J. Laneman, D. Tse, and G. W. Wornell, "Cooperative diversity in wireless networks: Efficient protocols and outage behavior," *IEEE Trans. Inf. Theory*, vol. 50, no. 12, pp. 3062–3080, Dec. 2004.

[32] M. Hasna and M.-S. Alouini, "End-to-end performance of transmission systems with relays over rayleigh-fading channels," *IEEE Trans. Wireless Commun.*, vol. 2, no. 6, pp. 1126–1131, Nov. 2003.

[33] M. Bocus, C. Dettmann, and J. Coon, "An approximation of the first order Marcum Q-function with application to network connectivity analysis," *IEEE Commun. Lett.*, vol. 17, no. 3, pp. 499–502, Mar. 2013.

[34] R. Morsi, D. Michalopoulos, and R. Schober, "Multiuser scheduling schemes for simultaneous wireless information and power transfer over fading channels," *IEEE Trans. Wireless Commun.*, vol. 14, no. 4, pp. 1967–1982, Apr. 2015.

[35] A. Castano-Martinez and F. Lopez-Blazquez, "Distribution of a sum of weighted noncentral chi-square variables," *TEST*, vol. 14, no. 2, pp. 397–415, Dec. 2005.

[36] M. S. Bazaraa, H. D. Sherali, and C. M. Shetty, *Nonlinear Programming: Theory and Applications*. New York: John Wiley and Sons, 2006.

[37] A. Cambini and L. Martein, *Generalized convexity and optimization: Theory and applications*. Springer, 2008, vol. 616.

[38] M. J. Powell, "Convergence properties of algorithms for nonlinear optimization," *Siam Review*, vol. 28, no. 4, pp. 487–500, Dec. 1986.

[39] A. D. Belegundu and T. R. Chandrupatla, *Optimization concepts and applications in engineering*. Cambridge University Press, 2011.

[40] I. Csiszár and G. Tusnády, "Information geometry and alternating minimization procedures," *Statistics and Decisions, Supplement Issue*, vol. 1, no. 1, pp. 205–237, 1984.

[41] Y. Sun, . Baricz, and S. Zhou, "On the monotonicity, log-concavity, and tight bounds of the generalized Marcum and Nuttall Q-functions," *IEEE Trans. Inf. Theory*, vol. 56, no. 3, pp. 1166–1186, Mar. 2010.

[42] S. Boyd and L. Vandenberghe, *Convex optimization*. Cambridge university press, 2004.

[43] M. Avriel, D. E., S. Schaible, and I. Zang, *Generalized concavity*. Siam, 2010, vol. 63.

[44] A. Prékopa, "Logarithmic concave measures and related topics," in *Stochastic programming*. Citeseer, 1980.

[45] M. Bagnoli and T. Bergstrom, "Log-concave probability and its applications," *Economic theory*, vol. 26, no. 2, pp. 445–469, 2005.